UCLouvain

École polytechnique de Louvain

Development and optimization of 3V class anode free cells

Author: **Neel Sanghvi**
Supervisor: **Alexandru Vlad**
Readers: **Jean-François Gohy, Joris Proost**
Academic year 2022–2023
Master [120] in Chemical and Materials Engineering

People calculate too much
and think too little.

- Charlie Munger

Acknowledgements

Firstly, I would like to thank the FAME+ organizing committee for giving me an opportunity to study the FAME+ Master and supporting me with the Erasmus Mundus scholarship.

I would like to begin by thanking Prof. Dr. Jan Philipp Hofmann and Dr. Till Frömling from TU Darmstadt, for inspiring me to look at electrochemistry and its applications from a deeper perspective. I would like to thank all the professors, scientists, doctoral students, and others who have helped me broaden my knowledge of materials science and of the related industries.

I am enormously grateful to Prof. Alexandru Vlad for offering me an opportunity to do my master thesis in his laboratory. I thank him for his deep insights about battery research and his course LCHM2260, which helped me immensely to build my fundamentals about battery technology. I also would like to thank Prof. Jean-François Gohy and Prof. Joris Proost for agreeing to be a part of my thesis jury. Completing this thesis would not have been possible without the exhaustive guidance of Dr. Shubhadeep Pal, Dr. Binson Babu and Dr. Xiaodong Lin. I also would like to thank Dr. Petru Apostol, Dr. Rambabu Darsi, Dr. Vasudeva Rao Bakuru, Dr. Gulshan Kumar, Xiaolong Guo, Robert Markowski and Géraldine Chanteux and other Vlad energy group members for their continued help and support.

I would like to thank my friends Ahsan, Endy, Nikita-Maria, Pavan, Prabhat, Prafulla, Priyatosh, Sergio, Vinit among others who made foreign lands feel like home. Finally, I am thankful to my parents, family and friends in India who have always believed in me and have motivated me to move forward.

Abstract

An exponential rise in battery demand for EV and energy storage system (ESS) applications has exposed the weaknesses of contemporary lithium ion battery (LIB) technology. Conventional LIBs suffer from low specific energies and high manufacturing costs, and currently dominating cathode materials make use of cobalt and nickel which suffer from multiple supply chain issues. Anode free battery (AFB) technology can potentially offer higher specific energies at a lower cost. Current AFBs suffer from low coulombic efficiency (CE) among other issues. This low CE causes a significant loss of active lithium with every cycle. Increasing AFB performance requires either increasing average CE or replenishing the lost active lithium. This project aims to study the optimization of $LiFePO_4$ (LFP) based anode free cells by means of developing a lithium reservoir on the copper anode substrate. The lithium reservoir can be used to replenish the active lithium, and the reservoir will be built using a sacrificial agent. In this work Li_4-PTtSA, a conjugated sulfonamide is examined for use as a sacrificial agent. To this end, a LFP - Li_4-PTtSA hybrid cathode is fabricated in an inert atmosphere. Modifications in the first cycle of a cell have been reported to have a strong influence on the cycle life. To this end, an 'intermediate rest step' has been tested for the first cycle of a lithium copper cell which increases the average CE by increasing the stability of the initial SEI. This has improved the cycle life of the cell by more than 100 %. Lithium half, lithium copper, anode free and powder cells have been used to study the behaviour of LFP, Li_4-PTtSA and the copper anode substrate. Galvanostatic cycling has been used for electrochemical characterization. Presence of a lithium reservoir increases the cycle life of an anode free cell by 40 % in the considered case. Li_4-PTtSA is concluded to be a potential sacrificial agent for anode free battery optimization.

Abbreviations

AFB	Anode free battery
AFC	Anode free cell
CAM	Cathode active material
CE	Coulombic efficiency
DEC	Diethylene carbonate
DMC	Dimethyl carbonate
DME	Dimethyl ether
DOL	1,3 - dioxolane
EC	Ethylene carbonate
EMC	Ethyl methyl carbonate
ESS	Energy storage system
EV	Electric vehicle
FEC	Fluoroethylene carbonate
GCD	Galvanostatic charge discharge
LCO	Lithium cobalt oxide ($LiCoO_2$)
LFP	Lithium iron phosphate ($LiFePO_4$)
LIB	Lithium ion battery
LMB	Lithium metal battery
LMO	Lithium manganese oxide ($LiMn_2O_4$)
LNO	Lithium nickel oxide ($LiNiO_2$)
Li	Lithium
LiDFOB	Lithium difluoro(oxolato)borate
LiF	Lithium fluoride
LiFSI	Lithium bis(fluorosulfonyl)imide
LiTFSI	Lithium bis(trifluoromethanesulfonyl)imide
LiPON	Lithium phosphorus oxynitride

Li_4-PtTSA	Tetralithium benzene-1,2,4,5-tetrayltetrakis((methylsulfonyl)amide)
NCA	Lithium nickel cobalt aluminium oxide ($LiNi_xCo_yAl_{1-x-y}O_2$)
NMC	Lithium nickel manganese cobalt oxide ($LiNi_xMn_yCo_{1-x-y}O_2$)
NMP	N-methyl-2-pyrrolidone
OCV	Open circuit voltage
SEI	Solid electrolyte interphase
SHE	Standard hydrogen electrode
SIB	Sodium ion battery
Sep.	Separator
TFEC	Bis(2,2,2-trifluoroethyl) carbonate

Table of contents

1 General Context

1.1 Introduction: Some background towards batteries

After commercialization in 1991 by Sony, Lithium ion batteries (LIBs) have become the dominant type of rechargeable battery system being used to operate portable electronics. For the past two decades there has been a continuously growing trend of electric vehicle and renewable energy systems adoption [1]. This is due to rapidly exacerbating climate change, geopolitical factors due to fossil fuel dependency and rising air pollution [2]. EV applications necessitate the use of batteries and the irregular power supply obtained from renewable sources like solar and wind requires the use of energy storage systems (ESS). Presently lithium ion batteries (LIBs) dominate the EV & ESS landscapes, and occupy a significant portion of the portable electronics energy storage market. Despite having become synonymous with the term 'battery', LIBs are subject to continuous research and development to make them smaller, lighter and better.

The modern lithium ion battery is a rechargeable energy storage device which makes use of reversible intercalation and deintercalation of lithium ions in the positive and negative electrodes. The device during its use, will alternate between two extreme states, the discharged and charged states respectively. **Figures 1.1 a**, **1.1 b** show the discharged and charged states of a lithium ion battery. During the charging process, an external potential difference is applied which causes the positive electrode material to oxidize and lithium ions move out of the electrode by deintercalation (delithiation). The negative electrode is reduced and receives lithium ions. During the discharge process, a potential difference is generated as the negative electrode is oxidized and the lithium ions move out. The positive electrode is reduced and it receives the lithium ions by intercalation (lithiation). The ratio of the number of lithium ions transferred into the +ve electrode during discharge to the number of lithium ions transferred out of the +ve electrode during charge is called the coulombic efficiency. A transfer of electrons between the electrodes through an external circuit accompanies this transfer of ions in order to maintain electrical neutrality of the system. This electron transfer creates a current which is used to power electrical and electronic devices. The positive and

negative electrodes of the battery during the discharge process are termed as ‘cathode’ and ‘anode’ respectively.

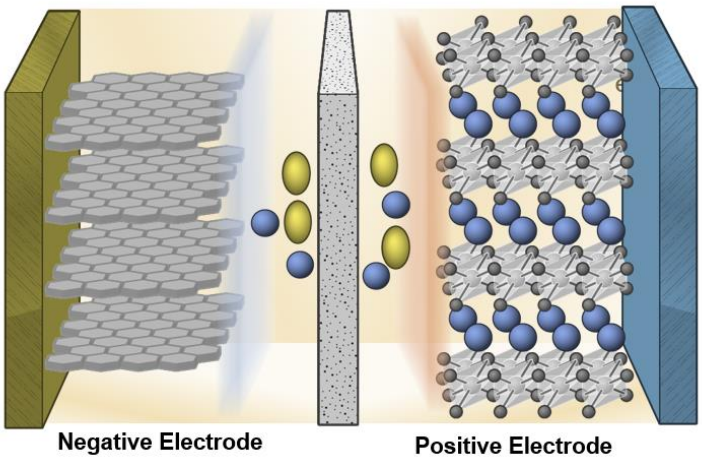

Figure 1.1 a: Lithium ion battery in discharged state.

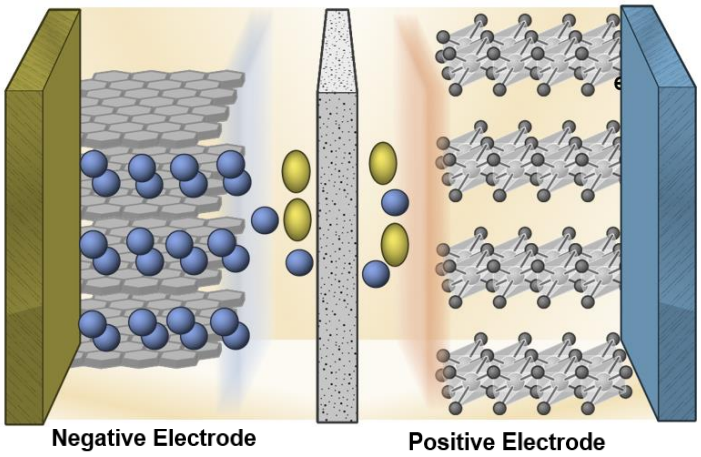

Figure 1.1 b: Lithium ion battery in charged state.

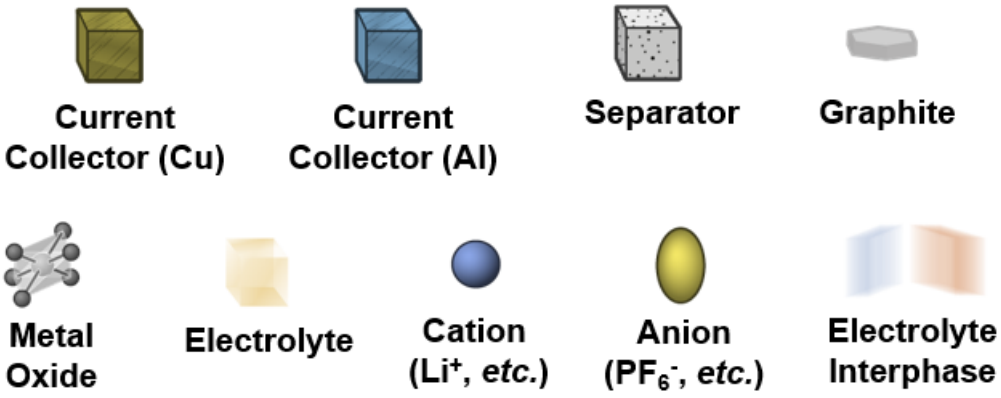

Figure 1.1 c: Materials/ Parts in a lithium ion battery.

Since the battery can be considered to oscillate between two extreme states, it is also called as a ‘rocking chair battery’. It can be very well said that the processes which allow lithium ion batteries to store and release energy correspond to the motion of individual lithium ions but the application of these processes is utilised on a much larger scale.

Even this scale has a very wide spectrum. On the smaller end of the spectrum are mobile phone batteries, for instance the battery of iPhone 13 Pro Max which has a capacity of 16.75 Wh. While on the higher end of the spectrum are ESS products. For e.g., the Tesla Megapack can store 3 MWh per unit.

1.2 What defines a ‘high performance’ battery?

It can be concluded from the previous section that lithium ion batteries and batteries in general play a fundamental role in our daily lives. Be it inside our watches and mobile phones or as a part of microgrids and heavy vehicles, batteries are everywhere around us and it is in the better interest of humanity and nature that academia and industry work together for the development of better, low cost and more sustainable batteries. But before going deeper into advanced battery systems and battery chemistries, it is important that answers to the following questions are understood very well:

1. What are the parameters to be considered when labelling a battery as ‘high performance’?
2. Which of these parameters are purely objective, and which are more subjective and open to interpretation?

Speaking from a broader perspective, parameters for battery evaluation can be directly linked to nuances in battery chemistry and battery architecture. Or they can be linked to how the battery reacts with the surrounding environment and to the operating conditions. This is especially true when developing batteries for use in rough/extreme conditions for e.g., abnormally high/low temperatures, maritime environments, etc.

One of the most important parameters with regards to battery performance is the specific energy of the battery E_D [Wh/kg]/[Wh/m^3], which refers to the maximum energy that can be stored in the battery on a unit weight or a unit volume basis.

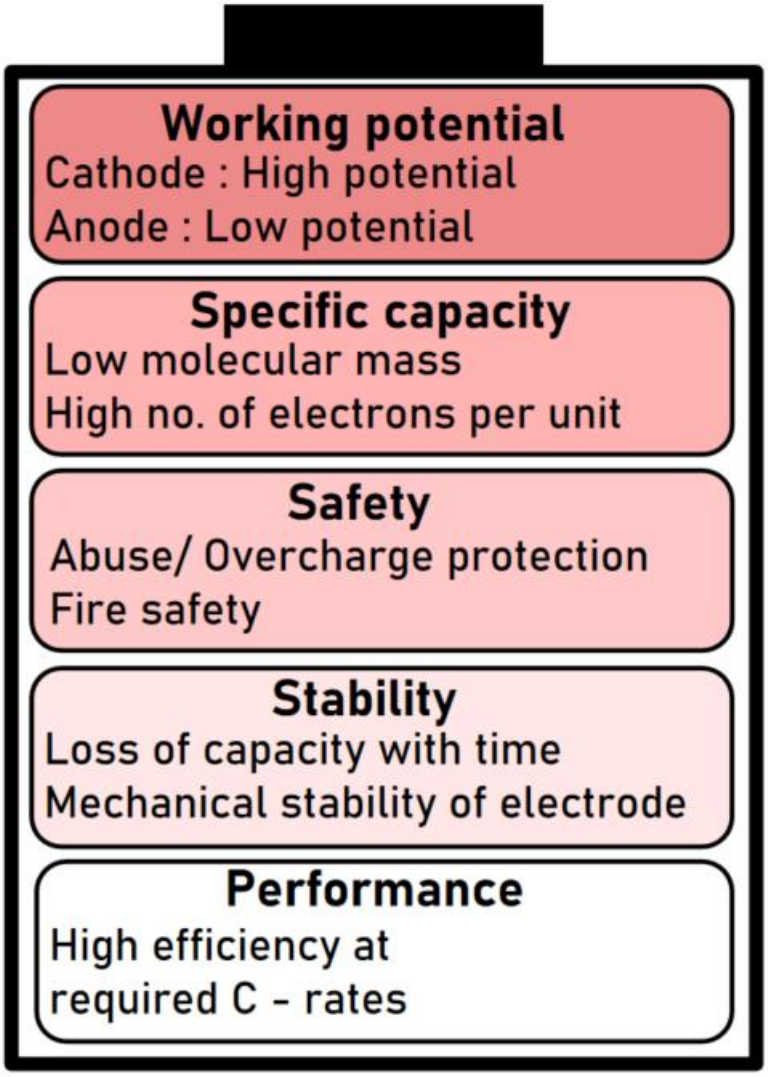

Figure 1.2: Parameters to be considered during development of high performance batteries.

In these cases, it is also called the 'gravimetric energy density' or 'volumetric energy density' of the system. For instance maximum cell level gravimetric energy density of the current LIBs is around 250 Wh/kg which puts a strong limitation on the current EV range [3].

$$\mathrm{E_D\ [Wh/kg]} = \mathrm{V\ [Volt]} \times \mathrm{C_{th}\ [Ah/kg]} \quad \text{(Equation 1.1)}$$

Equation 1.1 clearly shows that the specific energy is a function of the output voltage V [Volt] and the specific capacity of the material C_{th} [mAh/g]. The output voltage is calculated as the difference between the working potentials of the cathode and the anode. The specific capacity of an electrode material is the maximum amount of charge that can be stored in the electrode per unit mass. **Figure 1.3** shows the working potential and specific capacity values

for selected electrode materials. Thus, it can be concluded that in order to maximize energy density, it is imperative that chosen electrode materials have high specific capacities and give a high output voltage, resulting in cells with higher specific energies. For a perspective, as of 2018 the specific energy of commercial lithium ion batteries was typically less than 250 Wh/kg at the cell level [4]. Volumetric energy density of LIBs has increased by more than 8 times between 2008 and 2020 [5], but more improvement is needed in this area.

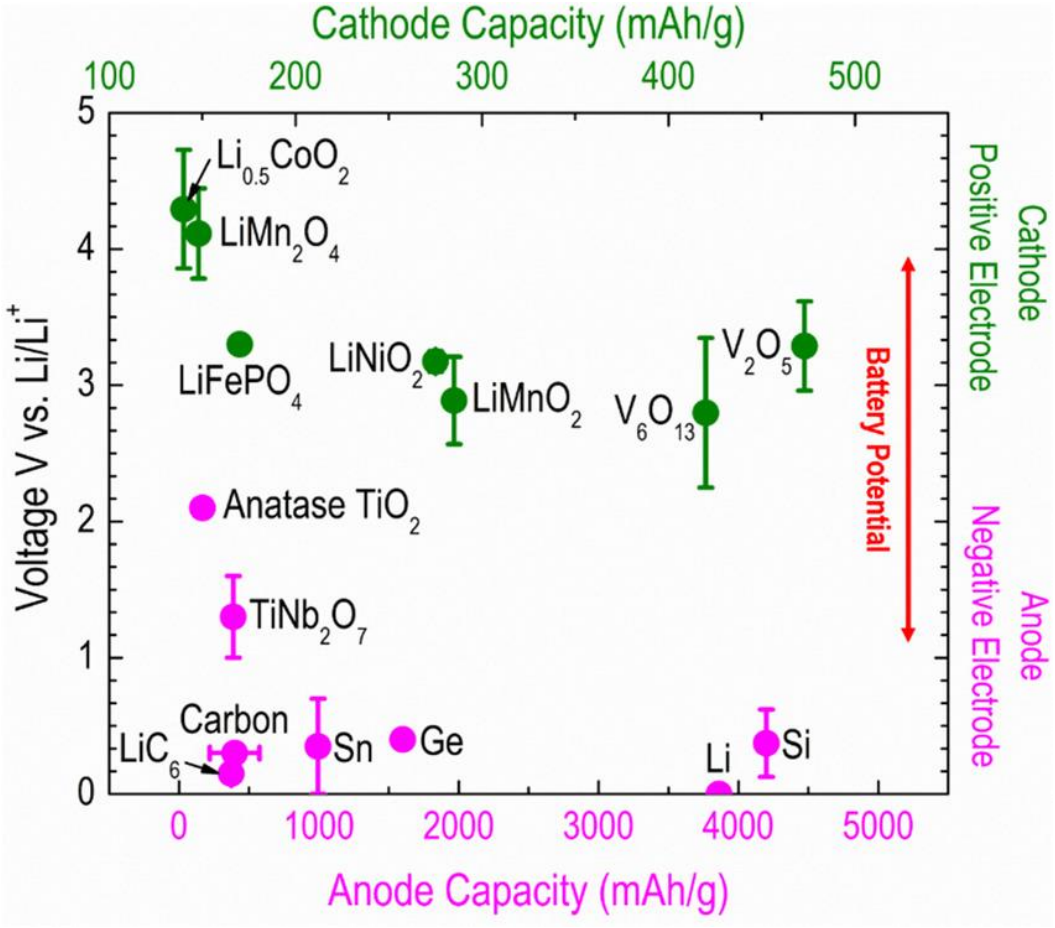

Figure 1.3: Working potentials and specific capacities for selected electrode materials. [6]

The specific capacity can be calculated with **Equation 1.2** where n is the number of electrons accepted/released per unit of the material, M is the molar mass of the electrode material, and F is the Faraday's constant having a value of 96485 C/mol.

$$C_{th}[mAh/g] = \frac{n \times F\ [C/mol]}{3600 \times M\ [kg/mol]} \qquad \text{(Equation 1.2)}$$

The above equation clearly reveals the major reason for lithium's high specific capacity. This is because lithium has the lowest molar mass among metals. Also, lithium has the highest magnitude of reduction potential at -3.04 V vs SHE.

On the other hand, there are various other factors which are subjective and open to interpretation. Such factors are either related to the choice of battery materials, the battery system or the operating conditions of the battery and the influence of the environment on battery performance. With the steep rise of lithium ion battery applications in the automotive industry, one of the major areas of concern for the industry and also a key cause of lack of confidence in electric vehicles (EVs) is the fire safety of a battery system [7]. Apart from the innovation needed in battery management systems, a major area of research for fire safety improvement is the battery chemistry. Development of electrolyte additives acting as fire retardants is an active research area. One of the more prominent battery chemistry related changes due to increased fire safety demands is the gradual shift from NMC based cathode systems to LFP based cathode systems for certain automobile segments, despite the lower specific capacity of LFP. The increased thermal stability of LFP is due to strong P-O covalent bonds which are absent in NMC, NCA cathode materials [8].

Safety has often been a key bottleneck for the commercial use of a given type of battery. In 1989, Canada based MoLi Energy was forced to issue a total recall for its rechargeable Li/MoS_2 lithium metal batteries (LMBs) after multiple fire incidents [9]. More recently, Apple had issued a battery recall for specific editions of the 15-inch MacBook Pro stating that the contained battery may overheat and explode. In 2022, there were numerous cases of electric scooters catching fire in India. They key cause of fires was determined to be the employed battery chemistry which was unfit for India's hot and sunny climate. In fact, the very motivation for LIB commercialization in 1991 was the disastrous MoLi Energy incident which convinced the community at the time that lithium metal anodes were inherently unsafe. Today operational safety is considered as a key parameter when comparing two battery systems (e.g., Li metal vs Li ion) or two choices for a battery component (e.g., LFP cathodes vs NMC cathodes).

Among other factors, careful attention must be paid to how battery performance is affected, by electrical abuse (overcharging/overdischarging) and by presence of irregularly varying loads for e.g., movement of an EV through a traffic congestion. The effect of such abnormal

operating conditions on the efficiency/life of the battery should be as low as possible. Also, a major area of research is the development of battery systems for optimal performance at extreme temperatures, which are required for niche EV applications in very hot or very cold places. Also, since a battery is used for a particular application for many cycles (1500-2000), it is necessary that the various interfaces inside the battery be stable with time. The stability of the electrode/electrolyte interface becomes very important here. This is one additional area in which LFP cathodes fare better compared to conventional NMC cathodes [10]. This lack of stability is one of the key barriers to the commercial use of LMBs, as the lithium metal anode/electrolyte interface is unstable and lithium metal undergoes a continuous reaction with the electrolyte leading to the formation of a high impedance SEI [7].

Since, batteries are an extremely application oriented system, it is important to understand the concept of C-rate. The C-rate is a measure of how fast or slow a battery is charged/discharged. A C-rate of 'x' implies that a completely discharged/charged battery will be completely charged/discharged in '1/x' hours. There is a strong demand from the automobile industry for fast charging batteries. But it has been proven that fast charging (high C-rate charging) of batteries degrades battery performance in terms of specific energy and specific power. Thus, it is imperative that suitable cathodes, anodes, and electrolytes are developed so that batteries show optimal performance for a longer life, even when used at high and variable C-rates.

1.3 High performance batteries: Current options

As discussed in the last section, specific energy of the battery is the landmark metric for evaluation of battery performance. Higher the specific energy of the system, higher is the amount of energy that can be stored per unit weight of battery, consequently more 'high performance' is the battery. **Figure 1.4** shows the evolution of cell level specific energies for Li-ion systems from 1991 to 2012. Current LIBs have specific energies of 240-250 Wh/kg or 550-600 Wh/l [11]. Focused research is needed to achieve the target of 500 Wh/kg or 750 Wh/l. Conventionally, innovation to improve specific energy has been focused on the system level or the component level. **Figure 1.5** shows multiple technologies which could potentially replace conventional LIBs.

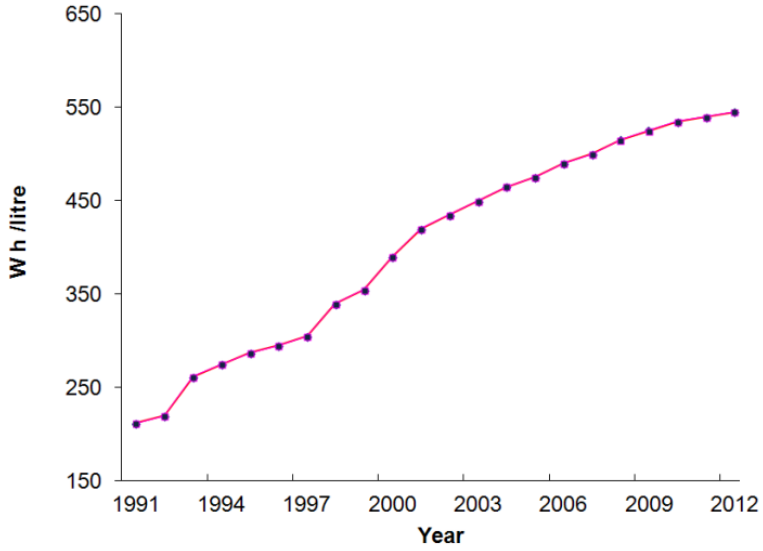

Figure 1.4: Evolution of cell level specific energies in the time period 1991 – 2012. [12]

The main basis for component level innovation is that the specific energy of the battery is a function of the specific capacity and working potential of the anode/cathode materials. Disappointingly, graphite which is also the most used anode material, has a specific capacity of only 372 mAh/g which results in current LIBs being heavy and bulky. This directly places a restriction on the range of an EV. There have been consistent efforts to incorporate silicon in the anode, either pure or in the form of a graphite composite as the specific capacity of silicon is ca. 4200 mAh/g, a more than 10 time increase from graphite [13].

In theory, a specific energy increase of ca. 60 % can be achieved with the use of silicon but the key issue is the volume difference between the lithiated and delithiated phases [14]. Another component level modification is to use a lithium metal anode (specific capacity ca. 3860 mAh/g) instead of a graphite anode, essentially the lithium metal battery, which was commercialized in the late 1980s only to be withdrawn in a short time due to multiple safety hazards [15].

Another major component level modification is to select cathode materials having higher specific capacity. The first lithium metal oxide material to be commercialized was LCO ($LiCoO_2$) in 1991, offering a specific capacity equal to a mere 135 mAh/g at a potential of 4.2 V vs Li^+/Li^0. It is important to note that optimized cathode materials must possess both, a

high specific capacity and a high working potential [16]. LNO ($LiNiO_2$) and LMO ($LiMn_2O_4$) were explored in depth but both these materials have substantial weaknesses.

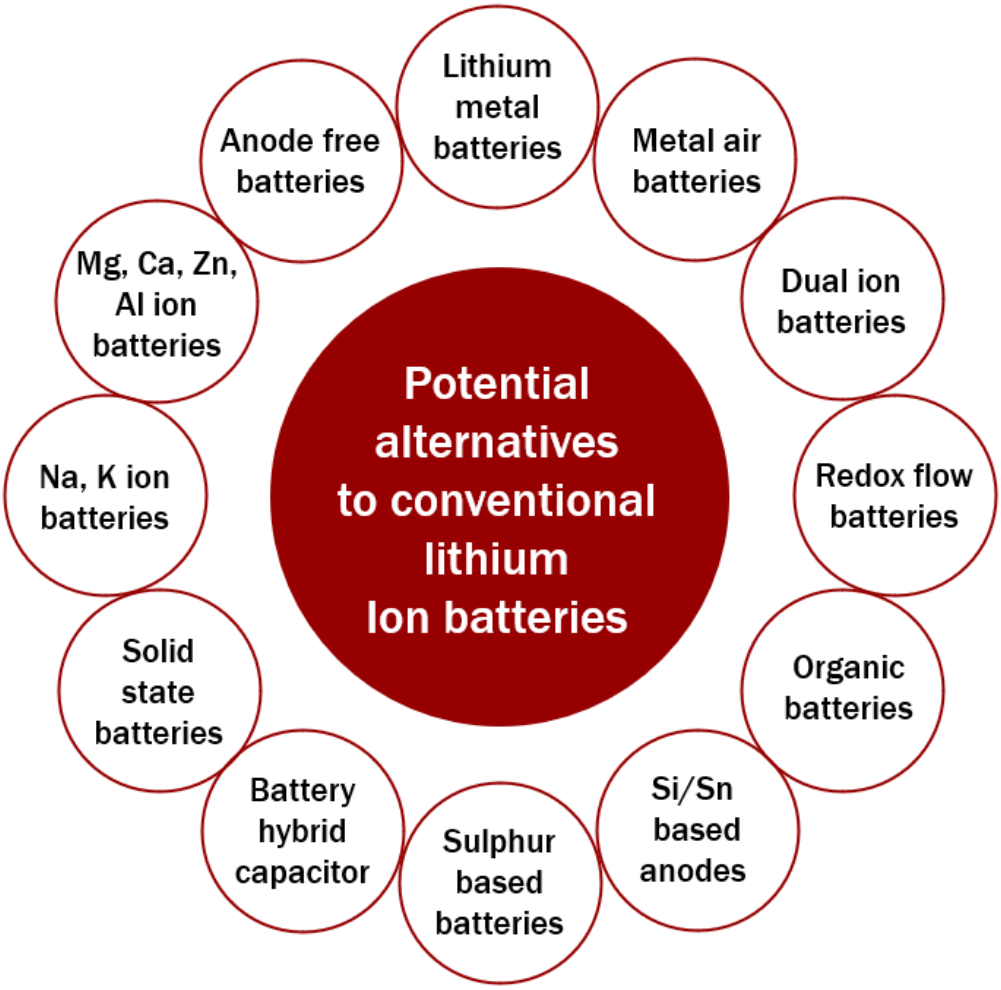

Figure 1.5: Potential alternatives to conventional lithium ion batteries.

With an aim to develop a superior cathode material by combining the strengths of LCO, LMO and LNO, NMC ($LiNi_{1-x-y}Co_xMn_yO_2$) was developed in the year 1999 which currently dominates the current cathode materials mix utilised in the market [17]. The specific capacity and working potential of NMC can be tuned by varying the ratios of nickel, cobalt, and manganese. Another cathode material being used in modern LIBs is NCA ($LiNi_{1-x-y}Co_xAl_yO_2$) which operates at an average potential of 3.7 V vs Li^+/Li^0 and gives a specific capacity of ca. 199 mAh/g for x=0.15, y=0.05 [18]. Finally, another cathode material that has a growing market share is LFP ($LiFePO_4$) which was discovered in 1997, and offers a specific capacity of 170 mAh/g at a working potential of 3.4 V vs Li^+/Li^0 [19]. The key advantage that LFP offers over other cathode materials is that it makes the battery manufacturing process free of cobalt, which conventionally faces issues when it comes to cost efficiency and ethical sourcing. But

in the end if we look at the specific capacities and working potentials of the available cathode materials (shown in **Figure 1.3**, **Page 5**), it can be concluded that innovation for cathode materials alone cannot help in achieving a cell level specific energy of 500 Wh/kg.

The other group of modifications has been focused on the system level. The are strong efforts to adopt post lithium systems based on Na, K, Zn, Al, Ca, Mg and other elements. A key hurdle for sodium ion battery (SIB) commercialization is the lack of low potential anode materials having high specific capacity. But despite their low specific energy (~200 Wh/kg), Chinese manufacturer CATL has decided to commercialize SIBs and Chinese automaker Chery has decided to start using them in their low budget EV models by the end of 2023 [20]. But other post lithium systems still face serious issues. Problems at hand for magnesium ion batteries are lack of suitable electrolyte chemistries and high performance cathodes [21]. Comprehensive studies on binders and current collectors are also required [22]. The general trend in this area is that these batteries are unlikely to be able to compete with LIBs in terms of specific energy. Moreover, these technologies are currently not mature enough for the community to be able to predict their commercial viability for the long term.

A disruptive set of concepts bearing the umbrella name of 'metal-air batteries' do promise a theoretical energy density much higher than that of LIBs. These systems presently suffer from multiple challenges in the cathode, anode and electrolyte areas, making commercialization in the short term an impossible task [23]. Li, Na and K-air batteries feature a non-aqueous electrolyte due to their highly reactive nature and the key issue limiting their performance is the formation of peroxides/superoxides on the air cathode. Zn, Fe, Al, Mg-air batteries feature aqueous electrolytes as these metal surfaces can be passivated to a certain extent by their oxides/hydroxides. Here the major issue is the polarization of the air cathode between charge and discharge which restricts the efficiency. For instance the efficiency of Zn-air batteries is unlikely to be higher than 65 % [24].

The Redox flow battery (RFB) represents an excellent set of technologies that has already achieved substantial market penetration. Characterized by a strong adoption for stationary energy storage purposes, it is plagued by low specific energies (< 125 Wh/L) which makes it unsuitable for automotive applications [25].

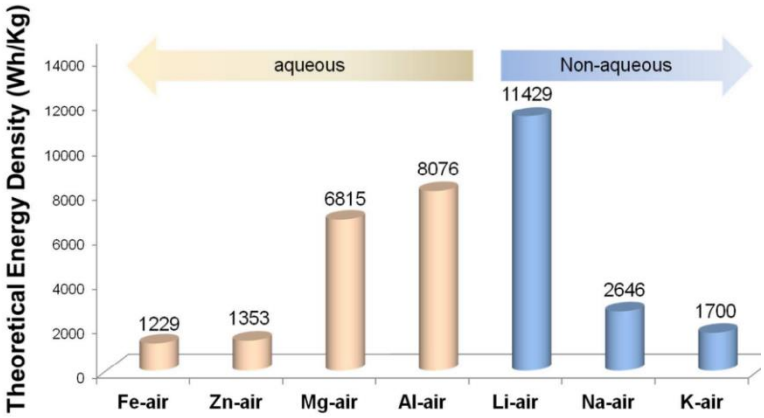

Figure 1.6: Theoretical energy densities for metal–air batteries. [23]
Note that metal-air batteries have the potential to offer much higher energy density (ca. 11500 Wh/kg for Li-air vs ca. 200 Wh/kg for Li-ion).

The anode free battery (AFB) is another interesting concept which offers an energy density that is substantially higher than that of the lithium ion battery, even surpassing the benefits offered by the lithium metal battery. This gain of energy density results from the elimination of the anode as the weight/volume occupied by the anode is reduced to zero. The copper current collector which is conventionally used as a substrate to build the graphite anode in a lithium ion battery, serves as a surface for lithium electroplating/electrodissolution. The intercalation/deintercalation processes at the anodic side in a lithium ion battery are replaced by lithium electroplating/electrodissolution processes in an anode free battery. However, it is important to note that the term 'anode free battery' is more of a misnomer as this concept is more akin to a zero excess Li anode metal battery. In a charged state, there is a lithium layer present on the copper anode substrate which can be said to represent an in-situ formed lithium metal anode. **Figure 1.7** shows the structural differences between a lithium ion, lithium metal and anode free battery.

From a product perspective, the anode free battery (AFB) can be viewed as a technology that has the potential to offer high specific energy at a lower cost as compared to the lithium ion battery. From the perspective of scientific development, anode free batteries constitute what are termed as 5th generation batteries. Current LIBs and lithium metal batteries (LMBs) can be termed as 3rd & 4th generation batteries. Out of the entire landscape of rechargeable energy storage systems, anode free batteries stand out as a viable upgrade from current lithium ion batteries. These batteries offer a strong advantage in the sense that the standard structure of a lithium ion battery is directly carried over to anode free batteries, without any substantial

distortion. Anode free batteries offer the highest specific energy for the intercalation anodes used in a lithium ion battery. The manufacturing and assembly processes are largely the same, the same anode substrate is used without actual anode manufacture. The elimination of the anode offers a significant cost advantage.

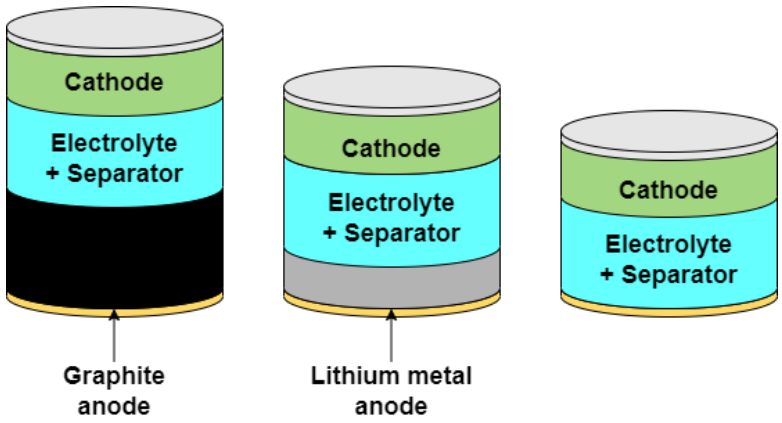

Figure 1.7: Differences in structure between lithium ion (L), lithium metal (C) and anode free batteries (R).

1.4 Anode free batteries: An overview

As seen in the previous section, anode free batteries (AFBs) appear as a feasible solution to the problem of lack of high performance batteries. With the first experiments performed in the year 2000, AFBs have a configuration of Al | LiXO | Sep. | Cu, unlike conventional LIBs which have a configuration of Al | LiXO | Sep. | C_6 | Cu. Here 'Sep.' denotes the separator and 'LiXO' denotes a standard lithiated oxide type cathode material e.g., LFP, NMC, NCA, etc. whereas C_6 denotes a graphite anode. Instead of a conventional anode, only an anode substrate is present.

The first AFB system was developed as solid state thin film battery with a LCO cathode and LiPON electrolyte [26]. Since then multiple initiatives have approached the anode free concept from non-conventional perspectives: sodium ion, solid state [27], thin film, niche cathode materials e.g., LiI, Li_2S [28]. The key advantage of an AFB over a conventional LIB or LMB is higher specific energy due to elimination of a conventional graphite or lithium anode. And since the graphite anode is replaced by an in-situ formed lithium metal anode, the output voltage is highest for the selected cathode.

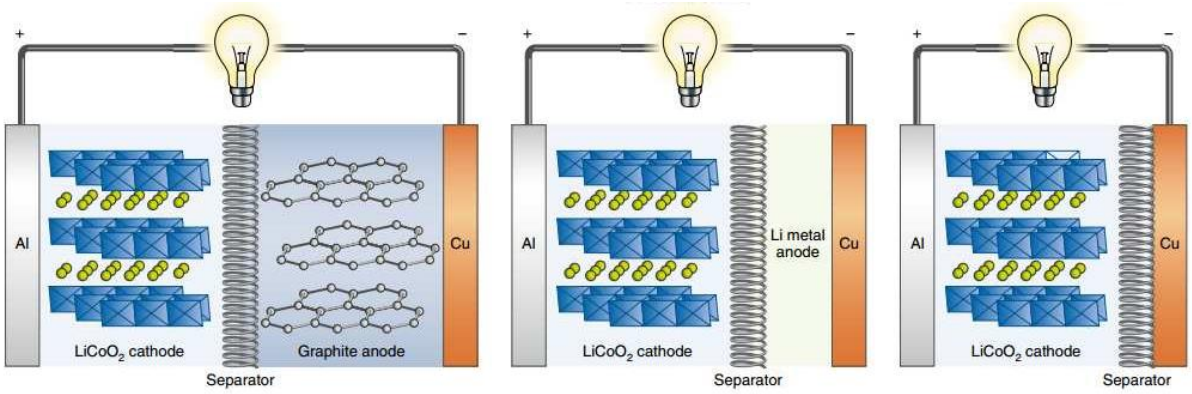

Figure 1.8: Conventional LIB (L), LMB (C) and AFB (R). [29]
Higher specific energy of an AFB results directly from the elimination of the anode.

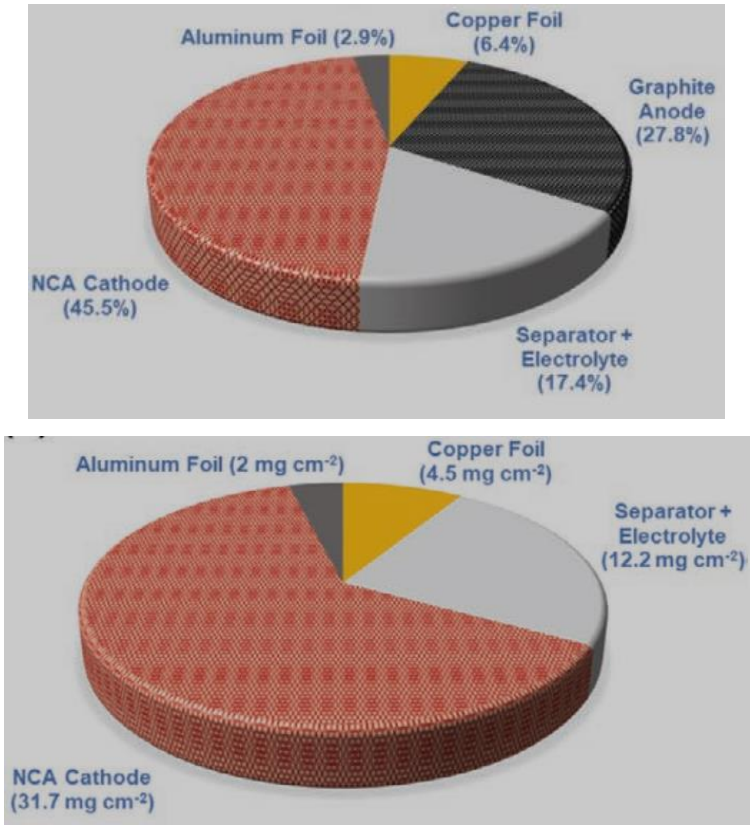

Figure 1.9: Differences in weight distribution for NCA based LIB (Top) and AFB (Bottom) systems. [30,31]

AFBs also offer cost and manufacturing advantages over LMBs due to absence of a lithium metal anode. Fabricating and handling lithium foils at a large scale while maintaining necessary microstructure and surface quality is a cost intensive process as an inert atmosphere is required, otherwise compounds like Li_3N, Li_2CO_3 and Li_2O are formed. In case of LIBs, considerable costs are involved in the sourcing and processing of battery grade graphite, AFBs fare better in this regard. In an as-assembled AFB, the cathode is lithiated and

the anode substrate is completely delithiated, 'self-discharge' is not possible which would otherwise lower the internal energy of the cell.

The major obstacle which does not allow successful commercialization of AFBs is low coulombic efficiency, which arises due to irreversible loss of capacity with each cycle (which also represents an irreversible loss of active lithium with each cycle). This is due to the poor quality of the electroplating/electrodissolution processes. Formation of dead lithium and weak SEI formation have also been cited as reasons for poor AFB performance [31]. Dead (mossy) lithium formation can be attributed to weak adhesion of deposited lithium on the anode substrate. In general, repeated electrodeposition of lithium on copper is known to be non-uniform, as shown in **Figure 1.12**. Weak SEIs suffer cracking and as a result, more lithium ions are consumed to form new SEI material [32]. Like lithium metal batteries, anode free batteries also suffer from dendrite formation at the anodic side. The formation of dendrites occurs due to irregular plating of lithium on the copper surface, which is caused due to irregular mass transport of lithium ions in the electrolyte [33]. This presence of dendrites (shown in **Figure 1.10**) poses a safety hazard due to increased risk of short circuits, as well as they cause unwanted reactions between lithium metal and the electrolyte which decreases the coulombic efficiency.

Multiple studies have focused on optimizing the constituents of the SEI with the aim of preventing unwanted electrolyte decomposition on the current collector surface. Multiple methods have been used for improving the efficiency performance of an AFB, these methods can be broadly grouped into three areas which are as follows [29,31]:

A. Modification of electrolyte
B. Modification of current collector surface
C. Modification of cell formation and cycling parameters

Another issue encountered during the operation of an AFB is the volume change of the system as the cell is charged and discharged. As the cell is charged, a lithium metal anode is formed in situ, increasing the width of the cell. As the cell is discharged, this anode is decomposed and the width of the system returns to the initial value, as shown in **Figure 1.11**. This change in volume must be compensated with some mechanism.

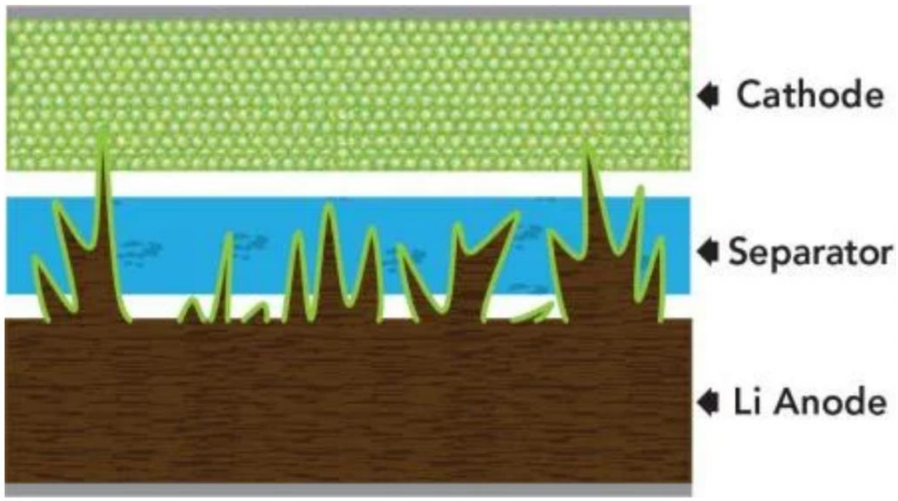

Figure 1.10: Dendrite formation and the increased risk of short circuits. [34]

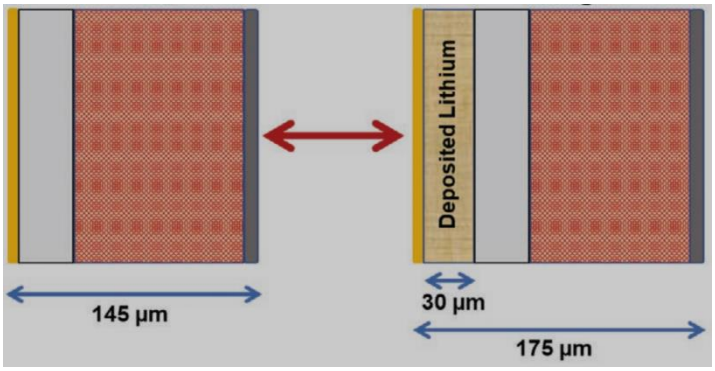

Figure 1.11: Volume change for an AFB between the discharged state (L) and the charged state (R). [31]

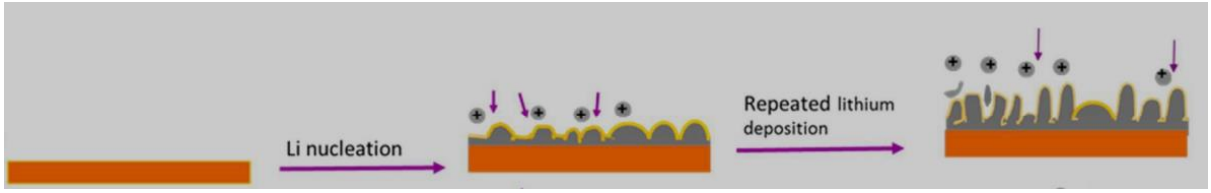

Figure 1.12: Repeated lithium electrodeposition of lithium on copper is known to be non uniform and can easily involve dendrite formation. [35]

1.4.1 Modification of electrolyte

Electrolyte composition and chemistry heavily influence the performance of a given anode free battery as the electrolyte components influence the morphology of the deposited lithium and also directly control the composition of the SEI formed on the copper anode substrate [36]. The SEI must possess two specific qualities: It must have high ionic conductivity with respect to lithium ions, and it must passivate the anode substrate surface to prevent further decomposition of the electrolyte [32].

It has been shown that LFP | Cu anode free cells assembled with $LiPF_6$ based carbonate electrolytes show poor performance [37]. This is chiefly due to reaction of the electrodeposited lithium with the electrolyte and $LiPF_6$ salt, forming a high impedance SEI. The plated lithium also tends to form dendrites and dead (mossy) lithium in presence of 1 M $LiPF_6$ in EC:EMC (3:7 wt:wt) carbonate electrolyte. This behaviour decreases the amount of active lithium in the system, leading to poor lithium transport reversibility and low coulombic efficiency. This behaviour was in agreement with prior observations regarding carbonate electrolytes [38]. On the other end LFP | Cu showed a superior performance with 4M LiFSI in DME electrolyte. Impedance of the cell during cycling was limited and the high CE achieved shows the high reversibility of the lithium electroplating/electrodissolution process. The increased concentration of the Li^+ ions in this case leads to a more uniform Li deposition on the current collector as can be seen in **Figure 1.13**. Formation of a lithium layer with large particle size (low surface area) is helpful for minimizing unwanted reactions between the electrolyte and lithium metal and it also minimizes presence of a fibrous structure which may lead to dendrite formation. FSI^- ions originating from the salt undergo reduction to form LiF which contributes to increased stability of the SEI. It is also observed that using an electrolyte having higher concentration increases the rate capability of the system. Ionic conductivity increases as the solvation forces between lithium ions and FSI^- anions are weak, resulting in better Li^+ transference number as compared to $LiPF_6$ based carbonate electrolytes [39,40]. It has also been reported in multiple studies that lithium metal has better compatibility with ether based electrolyte solvents (DOL, DME, etc.) when compared to carbonate type solvents [41,42].

Following these results, a dual salt electrolyte making use of a 2M LiFSI-1M LiTFSI in DME:DOL (1:1 vol:vol) in LFP | Cu anode free cells was reported [36]. It did not perform better than the earlier reported 4M LiFSI in DME electrolyte but here LiTFSI salt was also

used which is less expensive compared to LiFSI. Also, the total salt utilization per cell was lower which offers cost advantages. It was noted that the combined effect of the salts helps to build a more stable SEI. DFT studies were used to indicate that LiFSI has a higher tendency to decompose during cycling. FSI^- ions decompose and the products react with lithium metal deposited on the anode to form a stable SEI. XPS examinations of the cycled current collectors revealed the large presence of inorganic compounds Li_2CO_3, LiF and Li_2O as compared to 3M LiTFSI in DME:DOL (1:1 vol:vol). It was concluded that LiFSI salt stabilizes the SEI by improving composition due to increased formation of inorganic species, while LiTFSI salt provides ions for high electrolyte conductivity. Li deposition morphology was observed by SEM and it was smoother for dual salt electrolyte as compared to single salt electrolyte. As a combined effect of improved SEI and better electrolyte conductivity, the performance of the anode free cell was improved. This electrolyte composition of 2M LiFSI-1M LiTFSI in DME:DOL (1:1 vol:vol) is used for all the experiments in this work.

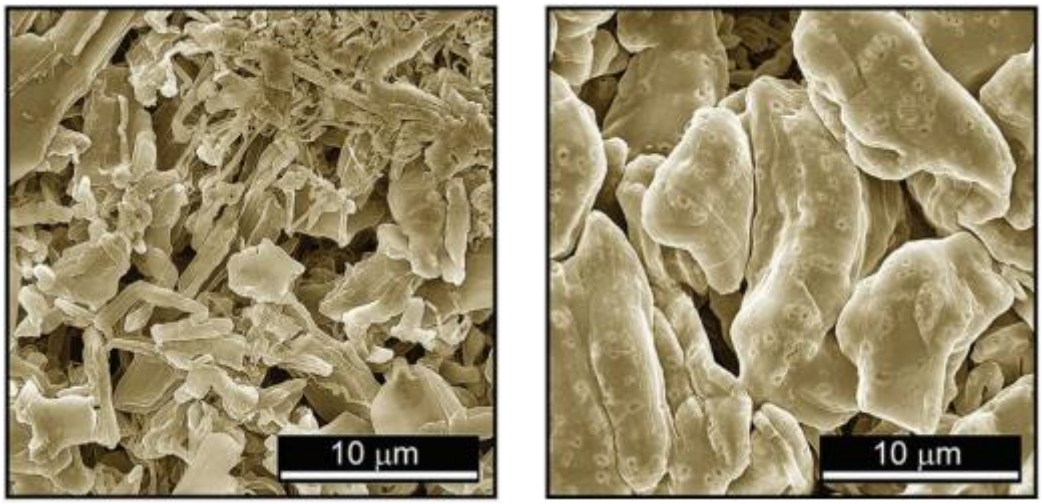

Figure 1.13: Lithium plating on copper current collector for first cycle in LFP | Cu anode free cells [37]. *For 1 M $LiPF_6$ in EC/EMC (3:7/ wt:wt) (L) a dendritic morphology is obtained whereas for 4M LiFSI in DME (R), a compact and nodular morphology is obtained*.

At this moment, more research is required to understand the ways in which electrolyte composition/concentration impacts SEI composition and stability. The fact that reversibility of the Li electroplating/electrodissolution processes is directly dependent on the properties of the SEI makes the situation more complex. Multiple research efforts have focused on LiF as a

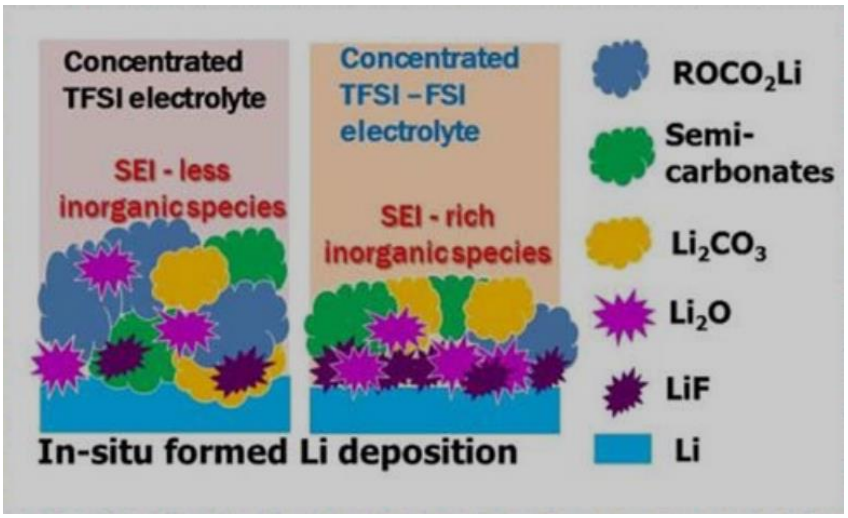

Figure 1.14: Comparison of SEI formed with $TFSI^-$ & FSI^- based vs only $TFSI^-$ based electrolytes: Electrolyte with $TFSI^-$ and FSI^- ions helps in formation of a stable and compact SEI, unlike electrolyte with only $TFSI^-$ ions. [36]

SEI stabilizing species. One direction is to focus on SEI stabilizing halides like LiI and the sulfide Li_3PS_4 which are known to have a high ionic conductivity. Polymeric and organic species must also be investigated. Development of relevant computational methods will go a long way when it comes to understanding SEI formation and SEI behaviour.

1.4.2 Modification of current collector surface

The morphology and composition of the current collector surface influences the nucleation and growth phases during the lithium deposition. The modifications that are done to current collectors can be grouped into two groups: in-situ and ex-situ. In-situ modification is chiefly done by electrolyte additives [43], while multiple approaches have been attempted for ex-situ modification.

Before going into the details of the current collector modifications, one must understand the key barriers that prevent uniform electroplating/electrodissolution of lithium on copper. One of the key factors which do not promote uniform deposition is the high nucleation potential for selected substrates [44–46]. This arises due to difference of crystal structure. Lithium is a BCC metal while copper used as a current collector has an FCC structure. But the difference of crystal structure can be compensated for when the deposition surface has an alloying behaviour towards lithium, decreasing the nucleation potential. Gold and tin are such metals

which show alloying behaviour towards lithium. The major issue with copper is the high nucleation potential due to lack of similar crystal structure and absence of alloying behaviour towards lithium.

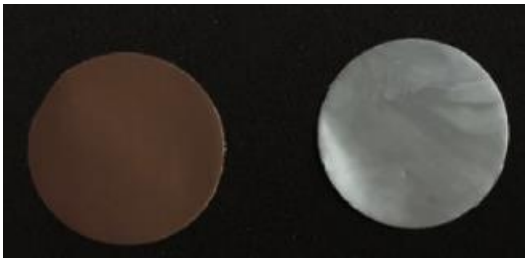

Figure 1.15 a: Bare copper anode substrate (L); Tin plated copper anode substrate (R) developed by electroless plating method. [47]

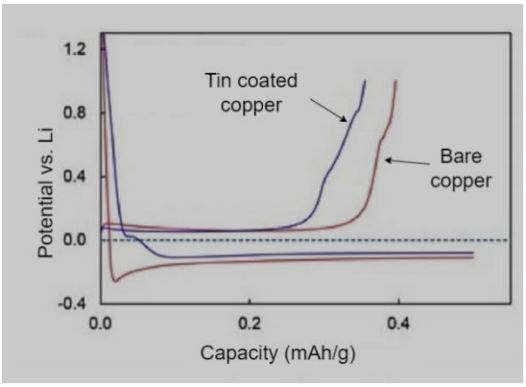

Figure 1.15 b: First cycle performed at 0.5 mA/cm^2: *Overpotential for Li || Sn plated Cu system is lower than that for Li || Cu system. First cycle capacity loss is higher for Li || Sn plated Cu system due to Li-Sn alloy formation. Li || Cu system does not undergo alloy formation.* [47]

One such study consisted of electroless plating pretreatment of copper current collectors to form a surface layer consisting of tin [47]. As compared to bare current collectors, cycle life increased from 30 to 80 cycles in NCA || Cu anode free cells with a $LiPF_6$ based carbonate electrolyte. Multiple studies have tried to improvise AFC performance by treating current collectors to form an artificial SEI. In one such study, $Li_7La_{2.75}Ca_{0.25}Zr_{1.75}Nb_{0.25}O_{12}$ (Garnet) was coated onto the copper surface by an electrospinning based method. This modification resulted in lower polarization and better capacity retention in NMC || Cu AFCs with a carbonate based electrolyte. Other studies have focused on artificial SEIs like PEO (Polyethylene oxide) and MLG (Multilayer graphene) [35,48]. For LFP || Cu based AFC with ether electrolytes, MLG treated current collectors exhibited better capacity retention at 50 cycles than the ones treated with PEO.

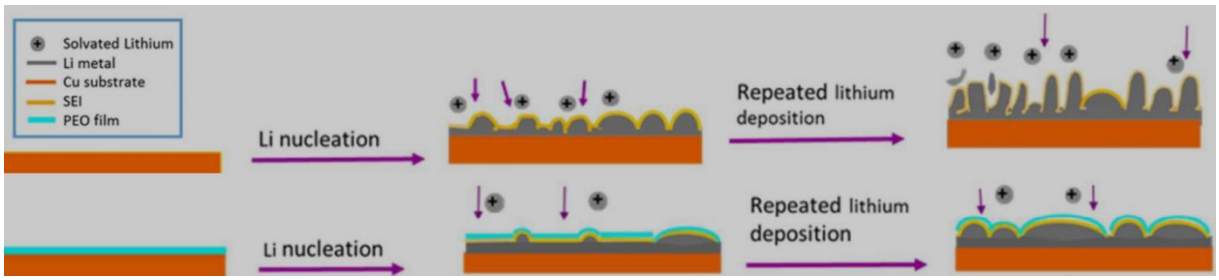

Figure 1.16 a: Schematic representation of differences in repeated lithium deposition for bare copper (Top) and PEO coated copper (Bottom) anode substrates. [35]

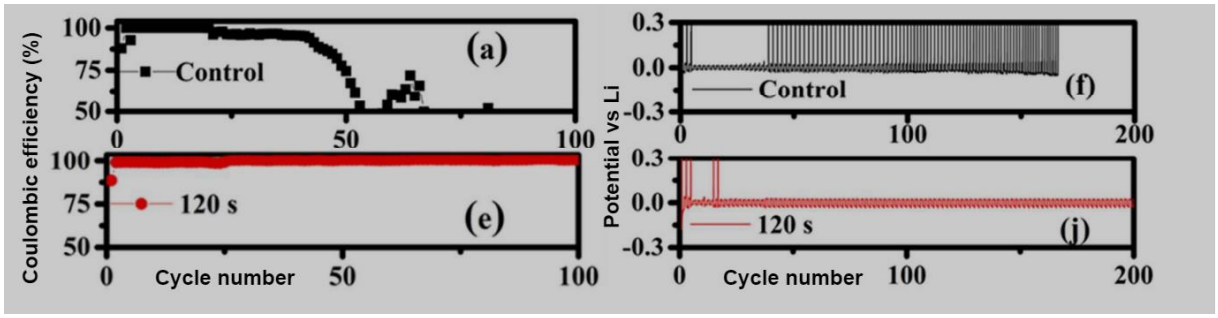

Figure 1.16 b: Differences in cycling performance of Li || Cu cells for bare copper (Top) and PEO coated copper (Bottom) anode substrates. PEO is coated by electrospinning process at 4000 rpm for 120 seconds. [35]

Until now, initiatives have almost exclusively focused on experimental methods for the identification of suitable current collector surfaces. But computational studies will make the entire process of finding and selecting substrates for lithium electroplating/electrodissolution much more efficient. It is important to note that the modification of current collectors may eventually act as a barrier to AFB commercialization as these treatments often make use of somewhat exotic methods like chemical vapor deposition (CVD), sputtering and electrospinning which are expensive and energy intensive processes to implement at a large scale, with some of these processes being very slow and time consuming.

1.4.3 Modification of cell formation and cycling parameters

The SEI is a crucial part of the battery during the operation stage, and is formed in-situ after the cell is assembled. It is desirable to have a stable and passivating SEI before the cell is cycled for the long term. On the other hand, since the first charge step involves a first plating of lithium on the current collector and formation of the SEI, the first cycle conditions also

have a significant impact on the long-term cycling stability of the cell. Multiple studies have shown the impact of the first cycle protocol on the long term performance of the cell [37,49–51].

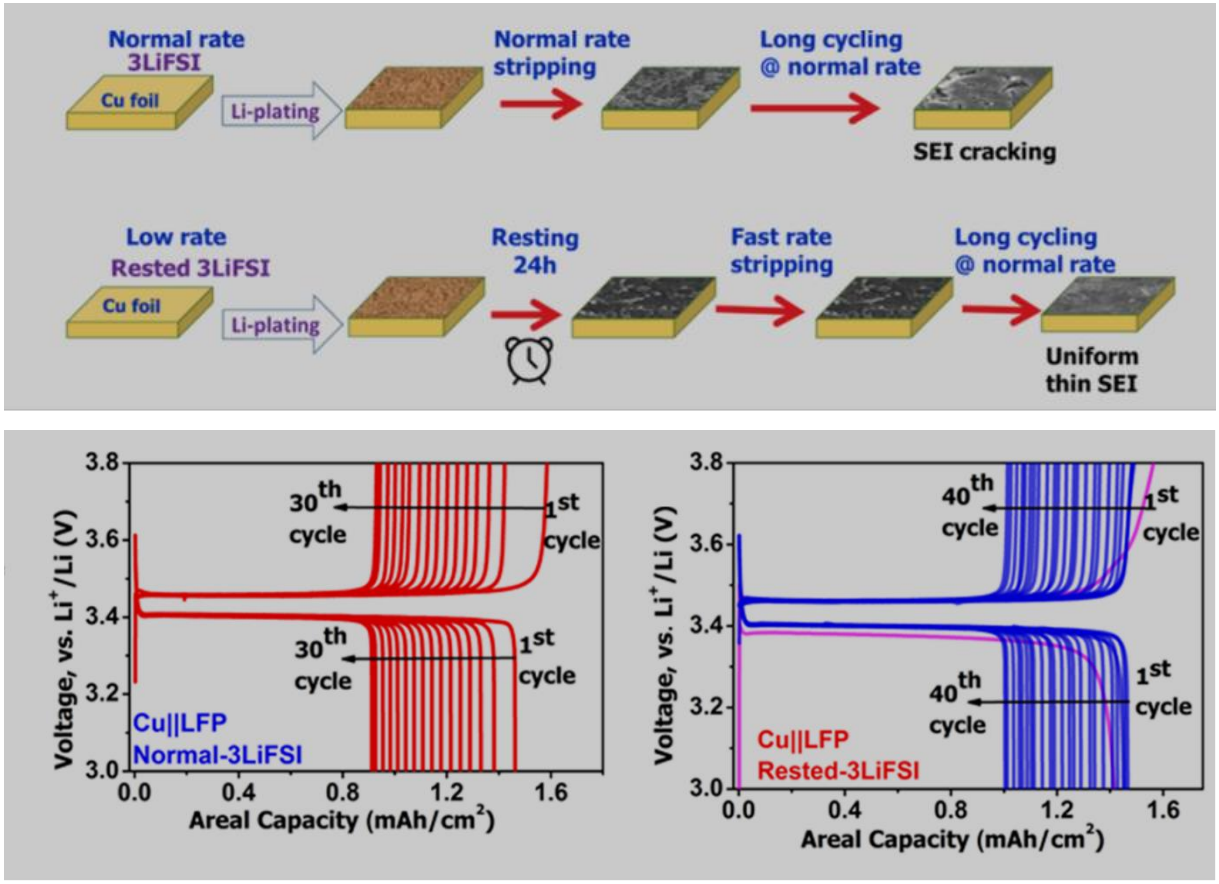

Figure 1.17: Introducing a rest phase and increasing the discharge current density in the first cycle protocol in case of 3M LiFSI in DOL/DME (1:1 v:v) improves SEI structure.
Top : Schematic showing difference in cycling protocols.
Bottom : Differences in capacity retention in LFP || Cu anode free cells for the two cycling protocols. [52]

An integrated first cycle and resting protocol was introduced to promote the formation of a robust SEI [52]. Post assembly, the cell was charged at a low rate to ensure lithium deposition at a slow rate. After this a rest period of 24 hours was given to allow for high quality SEI formation. Then the cell was discharged at a rate higher than the charge rate following which galvanostatic cycling was done at a low rate to study cell performance. The 24 hours rest period contributed to higher capacity retention compared to the case in which the rest period being absent, the first discharge was started directly after the first charge. This result is interesting and can be further investigated to develop more efficient first cycle protocols. Other than first cycle current rates and resting periods, other variables have also been evaluated. Application of mechanical pressures in the range of 75-2200 kPa during the first

cycle to improve long term capacity retention was explored for carbonate electrolyte solvent systems in NMC532 | Cu pouch type anode free cells [53]. SEM examinations were used to investigate the morphology of plated lithium and it was concluded that the application of pressure in general can lead to increase in initial plating efficiency. This is because the high pressure involved inhibits the mossy deposition of lithium.

It was also shown that as compared to a FEC:DEC electrolyte system, a FEC:TFEC system improves initial plating efficiency. Increased system temperature during the initial cycle was studied for NMC | Cu pouch type anode free cells with a 0.6 M LiDFOB - 0.6 M $LiBF_4$ in FEC:DEC (1:2 v:v) electrolyte [54]. It was reported that the long term cell performance of the cells at 20 °C under pressure increased by large margins when the first two cycles were performed at 40 °C, the number of cycles to 80% capacity retention increased from 18 to 60. This performance was further improved when the applied pressure was increased from 75 kPa to 2200 kPa. To summarise, elevated temperature and pressure during the initial cycles can be used to improve long term anode free cell performance by improving the SEI morphology and composition.

2 Scope and Objectives

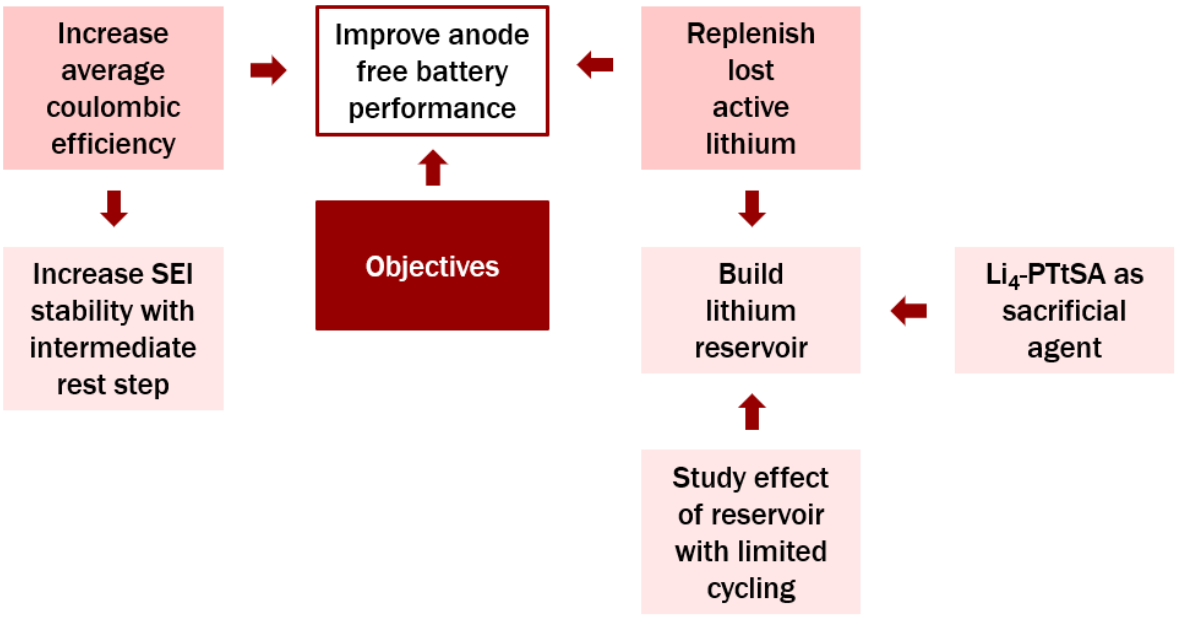

Figure 2.1: Overview for objectives of this work.

As explained in Chapter 1, anode free batteries do have consistent problems. The major problem is the low coulombic efficiency (CE) of the lithium electrodeposition/ electrodissolution processes on the copper anode substrate. There are two aspects to consider here.

The first aspect is that improving the average coulombic efficiency would lead to an improvement in anode free battery (AFB) performance. It is already established that the composition and quality of the solid electrolyte interphase (SEI) is an important aspect influencing long term battery performance. The SEI is formed during the first cycle of the cell when the lithium ions deintercalate from the cathode for the first time and approach the anode (copper anode substrate in an AFB). This means that the first cycle conditions can have an important effect on the SEI quality. The technique of giving a gap (a period of zero current) between the first charge & the first discharge to improve SEI formation has been reported in the literature. In this work the effect of having an 'intermediate rest step' or a 24 hour gap of

such type has been studied and it can be used as a method to improve long term CE for anode free batteries.

The second aspect is that a lower coulombic efficiency for a given cycle implies a higher active lithium loss for that cycle. This loss decreases the cycle life of the cell. One method to counter this to replenish the lost lithium with the help of a lithium reservoir located on the copper anode substrate. The broad idea is that a sacrificial compound embedded in the cathode generates lithium ions in the first cycle to form a lithium reservoir on the copper anode substrate.

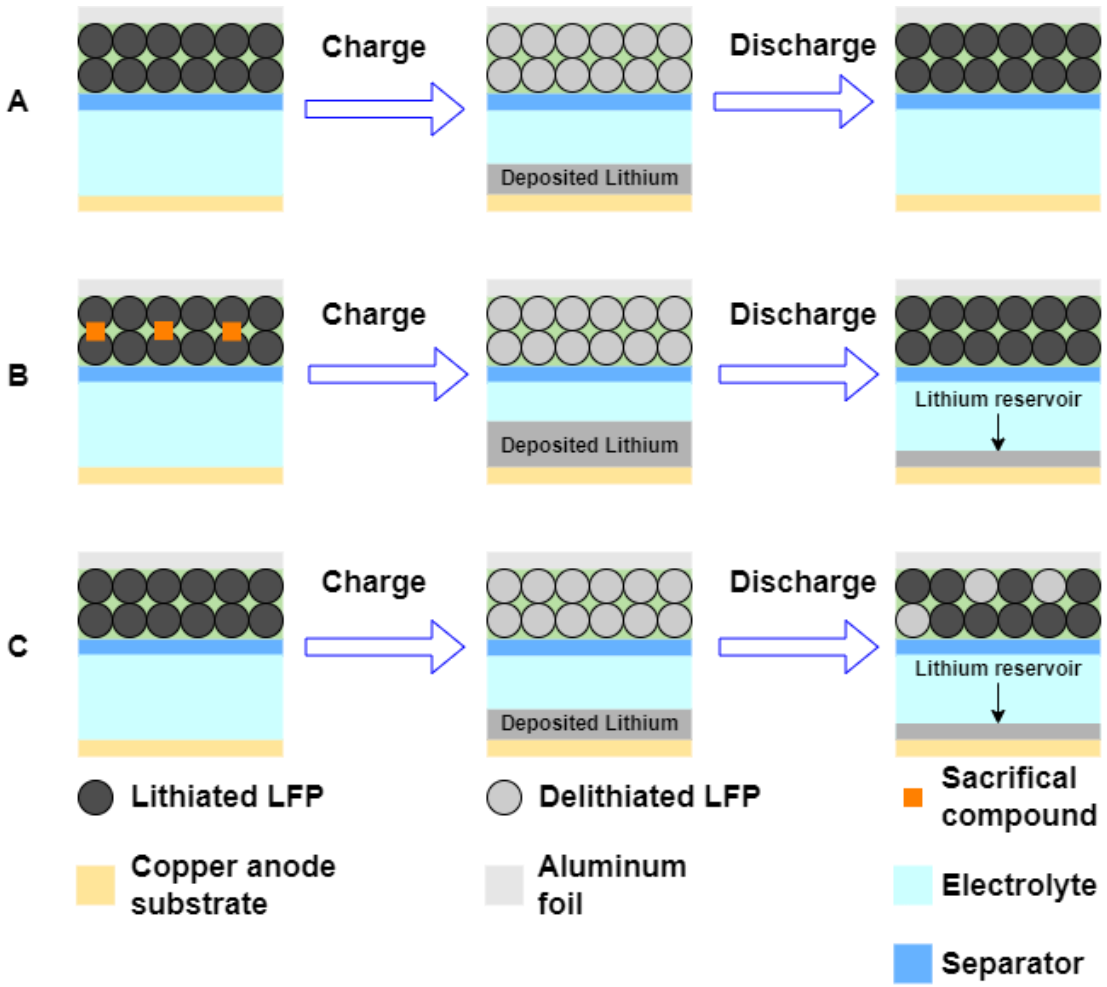

Figure 2.2: Modes of cycling for anode free cell:
Normal cycling with no formation of lithium reservoir (Top)
Use of sacrificial agent for formation of lithium reservoir (Centre)
Limited cycling for formation of lithium reservoir (Bottom)

The effect of the presence of a lithium reservoir on cell performance has been studied by making use of limited cycling to form a lithium reservoir in an anode free cell. A large gain

in cycle life has been realized. An overview of lithium reservoir formation by limited cycling and by use of a sacrificial agent has been given in **Figure 2.2**.

Regarding the choice of sacrificial agent for lithium reservoir construction, Li_4-PTtSA has been examined for use as a sacrificial agent. It is observed that NMP, the solvent for the cathode preparation process tends to partially dissolve Li_4-PTtSA, possibly resulting in phase separation. This unwanted behaviour requires more analysis for a thorough explanation and as of now, the cathode fabrication process requires a substantial improvement. But on a broad level, it is concluded that Li_4-PTtSA is a potential sacrificial agent for anode free battery optimization.

In the end, perspectives have been given regarding the next steps that can be taken in the short and the long term, regarding anode free battery optimization with the use of Li_4-PTtSA as a sacrificial agent.

3 Overview of Experiments

All experiments have been done primarily at the cell level, where the cell components (cathode, anode, and electrolyte) are prepared using standard laboratory methods. Multiple types of cells are used to understand potential methods to optimise anode free batteries. Lithium half cells, lithium copper cells, powder cells and anode free cells are used in this work. An overview of the experimental aspects of this work is shown in **Figure 3.1**. The experimental details can be broadly divided into the methods and materials sections. All the experiments done have been carried out at an ambient temperature (25 °C), and a dual solvent – dual salt electrolyte (2M LiFSI + 1M LiTFSI in DOL/DME (1:1 v:v)) has been used for all experiments.

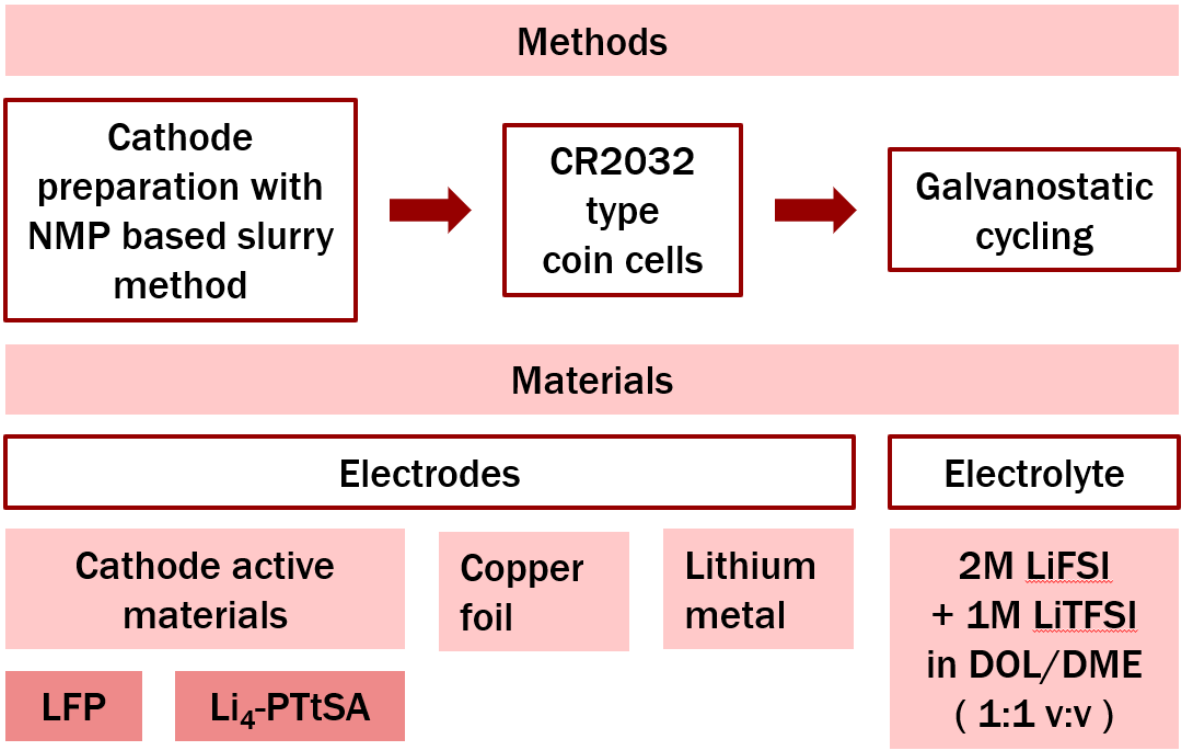

Figure 3.1: An overview for the experimental aspects of this work.

3.1 Overview of materials

3.1.1 Primary cathode active material

Lithium iron phosphate, $LiFePO_4$ (LFP) is a polyanion type cathode material which was first identified in 1997 [19] and it is currently used in multiple EV and ESS applications. Currently, the cathode active materials (CAM) market is dominated by NMC and NCA materials which make use of nickel and cobalt. These two elements suffer from multiple supply chain issues ranging from environmental and human impacts of mining to a volatile price environment. These factors have led the industry and academia to develop 'nickel and cathode free' cathode chemistries. LFP is one premier material in this group of chemistries. As of September 2022, the market share for LFP batteries in the global EV market was 31% [55] and this value is set to rise as patents have started to expire. With a theoretical specific capacity of 170 mAh/g and a working potential of 3.4 V vs Li^+/Li^0 [56] , LFP works with a biphasic delithiation process. Higher thermal stability due to strong P-O covalent bonds results in higher operational safety at the battery level [10]. Among other benefits, LFP offers cost benefits and a higher cycle life [57]. The low specific capacity of LFP against other chemistries currently limits its applications to ESS products and battery applications for low to medium range EVs.

3.1.2 Sacrificial agent

As outlined in Chapter 2, an alternative approach to improve anode free battery performance is to use an additive acting as a sacrificial agent to make a lithium reservoir on the anode substrate by the electrochemical in-situ deposition of lithium metal. On a broad level, multiple additives have been explored so far to improve battery performance in general, e.g., Co/Li_2O [58] and $LiFeO_2$ incorporated Li_2MoO_3 [59]. The general concept is to use the cathode additive as a sacrificial compound to generate lithium ions which can compensate for the loss of active lithium at each cycle. One recent study focused on the use of lithium oxalate ($Li_2C_2O_4$) as a sacrificial compound [60] for increasing the life of NMC based anode free cells. The idea here was to decompose $Li_2C_2O_4$ in the first cycle to form Li^+ ions, which can be deposited on the anode substrate to behave as a lithium reservoir for the subsequent cycles. The details of selected cathode additives/sacrificial compounds studied in the past have been summarised in **Table 3.1**.

An ideal cathode additive must yield lithium ions within a narrow potential window which is outside the standard operating window for the given cell. A narrow potential window implies a near-constant potential Li^+ ion release process. As it can be seen in **Table 3.1**, many previously tested additives generate Li^+ ions over a wide potential window.

Table 3.1: Overview of recently studied cathode additives.

Additive	Potential vs Li^+/Li^0 (V)	Charge capacity (mAh/g)	Reference
$Li_2C_2O_4$	4.5 – 4.9 V (Oxidation)	532	60
Li_2MoO_3	2.3 – 3.0 V (Delithiation)	244	59, 61
0.8 Li_2MoO_3 – 0.2 $LiFeO_2$	2.3 – 3.0 V (Delithiation)	221.7	59
Co/Li_2O (3:4 molar ratio) Nanocomposite	2.5 – 4.1 V (Delithiation)	619	58

For an LFP cathode, the cell has a standard operating window of 3.0 – 3.8 V vs Li^+/Li^0. This implies that any additive that is selected, must yield lithium ions in a window outside 3.0 – 3.8 V. Preferably, the ions must be generated at a potential lower than the operating window. For instance, if lithium oxalate were to be used as a cathode additive for an LFP cell, the cell would have to be subjected to a high potential of 4.7 V vs Li^+/Li^0 only for the purpose of generating a lithium reservoir. This would result in a complicated formation/ageing procedure. Thus, for an LFP cell, it is strongly recommended to use an additive which generates Li^+ ions below 3.0 V vs Li^+/Li^0.

And, it is highly desirable that the selected additive does not contain any metal that is not originally present in the cell as this would lead to additional complications for battery recycling, which is becoming more important day by day and which is already a complicated process. For instance, the use of Li_2MoO_3 as a cathode additive for any given purpose would introduce molybdenum in the battery system. Battery recycling for such type of batteries would require a separate process for molybdenum recovery.

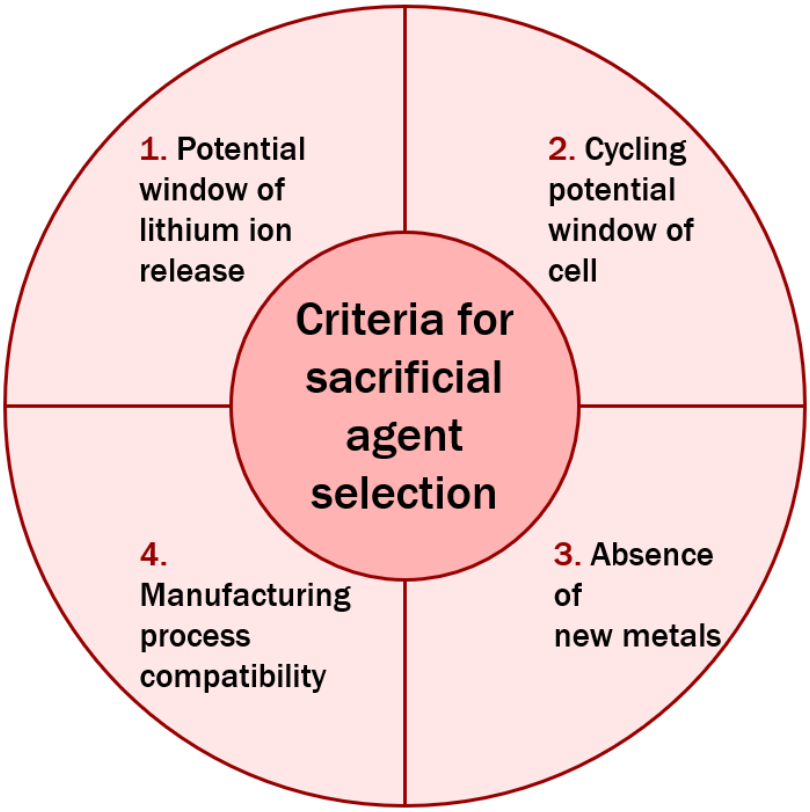

Figure 3.2: Overview of criteria for sacrificial agent selection.

Lithium oxalate ($Li_2C_2O_4$) was used as a cathode additive to increase the cycle life of NMC based anode free cells by lithium reservoir formation [60], but the oxidation of the $Li_2C_2O_4$ molecule involves evolution of CO_2 gas, which reacts further with lithium from the electrolyte and the cathode material to form Li_2CO_3 SEI layers. This entire process requires the consumption of lithium and requires a high potential of 4.7 V vs Li^+/Li^0. Also, due to efficiency reasons all the CO_2 gas may not react and this may lead to the accumulation of gas inside the cell.

Cobalt – lithium oxide nanocomposites have been used as cathode additives to increase the life of LFP – graphite full cells [58] but using this specific additive goes against one of the basic motivations to move to LFP based systems from NMC and NCA based systems. One of the basic ideas about adopting cobalt free systems e.g., LFP is that battery manufacturers can become immune to the numerous issues related to the supply chain and ethical sourcing of

Cobalt. Thus, it can be said that it is quite befitting that any cathode additive selected for an LFP based system be free of cobalt and nickel.

Finally, an important part of selecting a sacrificial agent is considering the manufacturing process compatibility. Currently, cathode manufacturing utilises a slurry-based coating process with N-Methyl-2-pyrrolidone (NMP) as a solvent. The coating must be vacuum dried at 110 °C for complete NMP evaporation in order to obtain a solid coated cathode. These conditions imply that the selected sacrificial agent must be completely stable in contact with NMP as well as be stable at high temperatures up to 110 °C. An overview of the criteria for sacrificial agent selection has been given in **Figure 3.2**.

As we have seen, the key requirement for a sacrificial agent is that the redox potential must be located outside the routine potential window of cell operation. This window for an LFP cell is 3.0–3.8 V vs Li^+/Li^0 (Working potential of LFP is 3.4 V vs Li^+/Li^0). Keeping this and the other selection criteria in perspective, Li_4-PTtSA appears to be a sacrificial agent which could potentially be used to optimise LFP anode free cell performance via lithium reservoir formation.

Tetralithiumbenzene-1,2,4,5-tetrayltetrakis((methylsulfonyl)amide)[Li_4-PTtSA] is a type of conjugated sulfonamide which is an organic battery material and has a redox potential of 2.75 V vs Li^+/Li^0 [62] in solid phase and has a specific capacity of 120 mAh/g with a molar mass of 474 g/mol. The structure of the molecule has been shown in **Figure 3.3**.

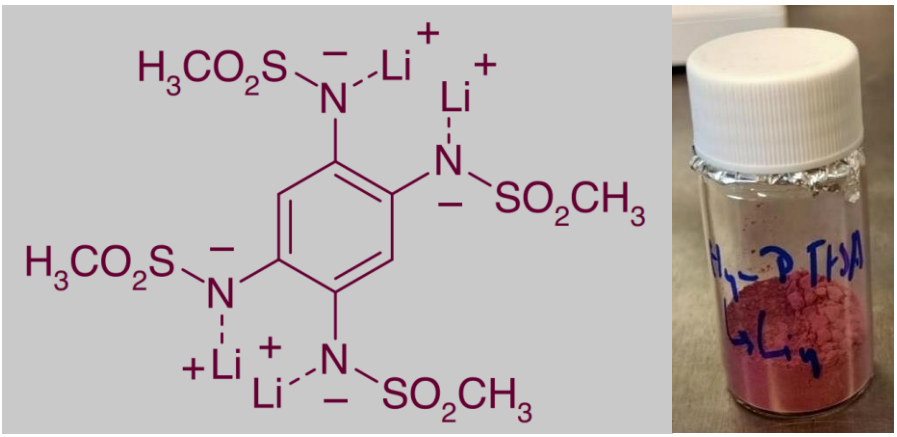

Figure 3.3: Molecular structure of Li_4-PTtSA [62] (L),
Li_4-PTtSA Sample (R).

The redox reactions can be given as follows:

$$Li_4\text{-PTtSA} \rightarrow Li_2\text{-PTtSA} + 2Li^+ + 2e^- \qquad \text{(Oxidation)}$$

$$Li_2\text{-PTtSA} + 2Li^+ + 2e^- \rightarrow Li_4\text{-PTtSA} \qquad \text{(Reduction)}$$

A powder cell is used to understand the energy storage capability and redox behaviour of Li_4-PTtSA, and it can be clearly seen that oxidation takes place within a very narrow potential window which is located below the LFP cell operation window of 3.0-3.8 V. The galvanostatic cycling data has been shown in Section 6.1 of the Supplementary information. Li_4-PTtSA contains only lithium among metals, and no new metal is introduced in the cell which would require a separate recovery process during recycling. Thus, it can be said that Li_4-PTtSA may act as a potential sacrificial agent for LFP anode free cell optimization.

3.2 Overview of methods

CR2032 type coin cells are used to observe multiple of types of energy storage systems in order to understand the behaviour and performance of LFP and Hybrid cathodes and the copper anode substrate. With regards to cathode preparation, a standard slurry-based coating method is used with aluminium foil as the cathode substrate. LFP cathodes are prepared in an ambient atmosphere while hybrid cathodes are prepared in an inert atmosphere inside a glove box and are never exposed to air. For electrochemical characterisation, galvanostatic charge and discharge is used. Standard cell assembly processes are used to assemble the cells.

3.2.1 Use of coin cells to understand energy storage behaviour

CR2032 type coin cells are constructed with different types of cathodes and anodes in order to understand the nuances of anode free batteries. Exploded views of the constructed cells are shown in **Figure 3.9** on Page 37.

A lithium half cell (henceforth referred to as Li half cell) is a system which resembles a typical lithium metal battery, with a polished lithium chip used as the anode. The choice of lithium as the anode material makes the potential at the anode equal to 0 V vs Li^+/Li^0. This allows us to understand the behaviour and performance of the cathode active materials, LFP and Li_4-PTtSA, as well the quality of cathode manufacturing. A lithium copper cell

(henceforth referred to as Li Cu cell) does not represent any potential type of battery, but it is a system which is used to study electroplating/electrodissolution of lithium on a copper surface as the system is charged/discharged. An anode free cell is a system which resembles a typical anode free battery. The conventional graphite anode of a lithium ion battery is replaced by a copper foil anode substrate. The basic differences in the structure of the cells can be seen in **Figure 3.4**. It can be clearly observed that the intercalation/deintercalation processes at the cathode in a lithium half cell and lithium electroplating/electrodissolution processes at the copper surface in a lithium copper cell occur together in an anode free cell to give a reversible energy storage behaviour. The lithium half and lithium copper cells allow us to understand the cathode and anode processes occurring in an anode free cell individually.

A powder cell is a crude arrangement in which the cathode lacks a substrate and consists of only of a powdered mixture in which the active material is the major component. This type of cell uses a glass microfiber separator and provides information about the behaviour of the active material.

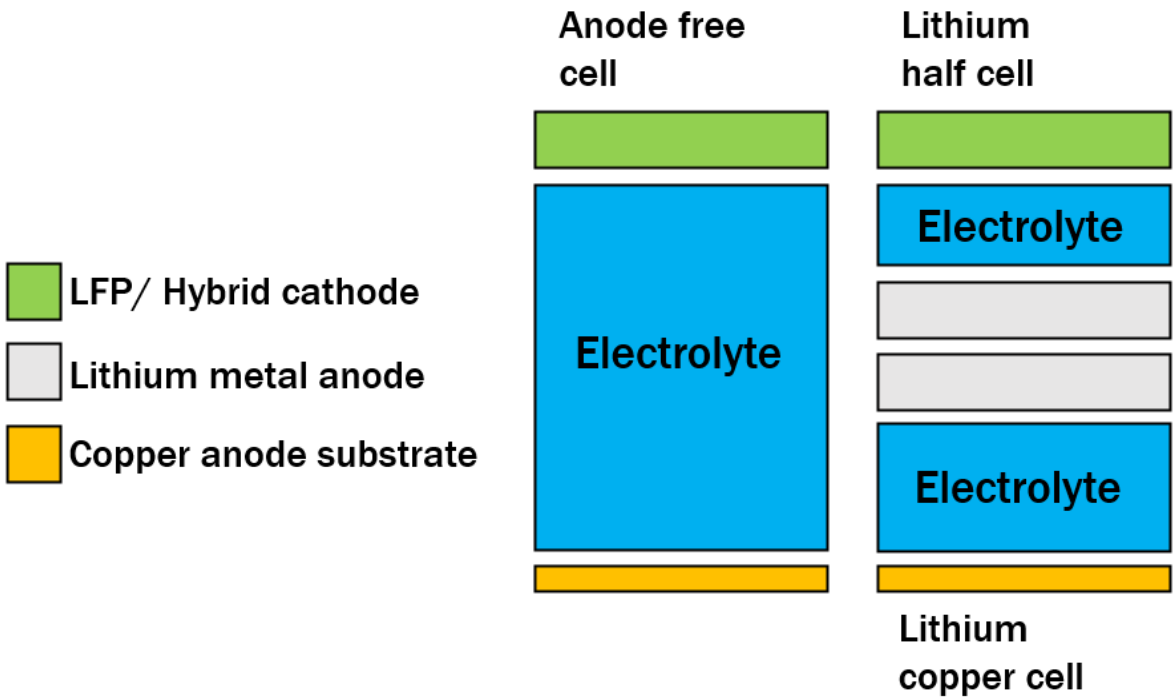

Figure 3.4: Schematic representation of anode free, lithium half and lithium copper cell.

3.2.2 Cathode preparation

3.2.2A LFP cathode preparation

Inorganic cathodes use only LFP ($LiFePO_4$) as an active material and aluminium foil (MTI, 25 micron) is used as a cathode substrate. PVDF (Kynar brand, Arkema) binder is mixed with calculated amount of NMP (Thermo scientific, 99%+) in a vial and is stirred using a magnetic stirrer (Arex digital PRO) and a stirrer bar for a minimum of 20 hours until a homogenous colourless solution is formed. Using a spatula and an agate pestle & mortar, carefully weighed amounts of LFP (Johnson Matthey) and C65 (Imerys) are mixed to form a smooth mixture. The mixed powder is then carefully transferred to the vial and this final mixture is subjected to stirring for a period of 24 hours, forming a smooth and viscous slurry. The ratio of the active material to C65, binder is 8:1:1 (by weight).

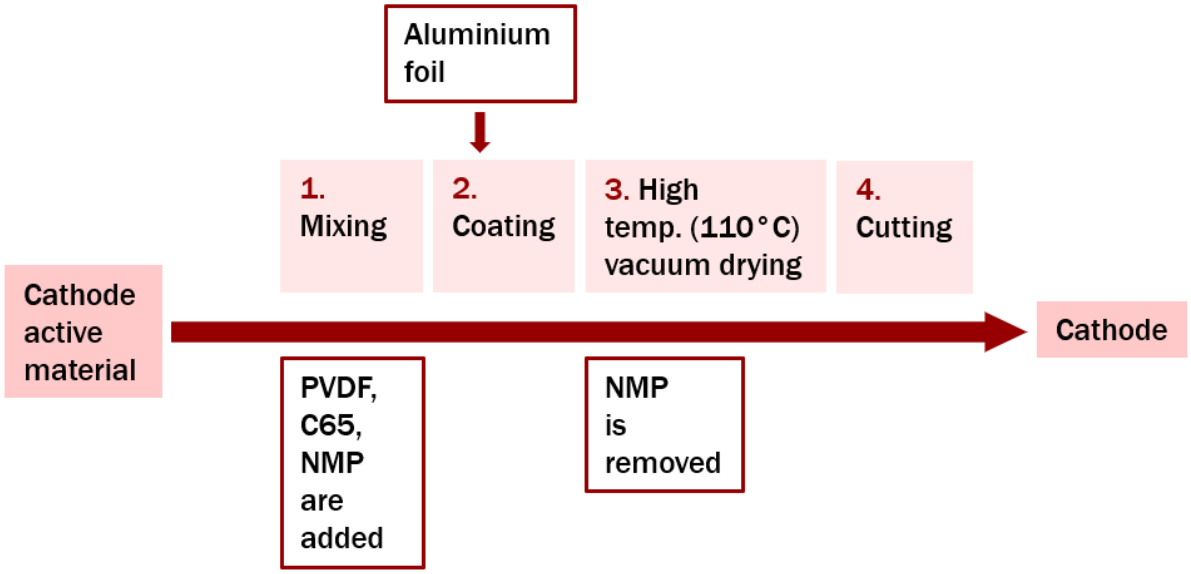

Figure 3.5: Basic overview of processes involved in cathode preparation.

A sheet of aluminum foil is prepared by cleaning with ethanol and drying in air. The foil has a rough side which appears dull and a smooth side, which appears bright. The rough side is used for the coating process. Using a vacuum coater (TOB VFC-300) a coating of 100 micron thickness is prepared on the foil with the prepared cathode slurry using a coater bar under the fume hood. The composition of the slurry can be found in **Table S1**, in Section 6.3 of the supplementary information. It must be noted that all processes involving NMP are carried out

inside a fume hood to minimise any health hazard caused due to evaporated NMP. The coating is allowed to settle for 15 minutes under the force of the vacuum after which the foil is transferred to an oven (VWR Dryline) for air heating at 70 °C for 1.5 hours. After this, the foil is moved to a vacuum oven (PCD C6-5000) for vacuum heating at 110 °C for 22.5 hours.

After this heating/drying process the foils are adequately cooled and cut into circles having 13 mm diameter using a hand cutting machine (EL-CELL, EL-cut). Weighing paper is used during the cutting process so that the electrodes are not damaged in any way. They are dried adequately in vacuum at 70 °C before they are transferred to the glove box for cell assembly.

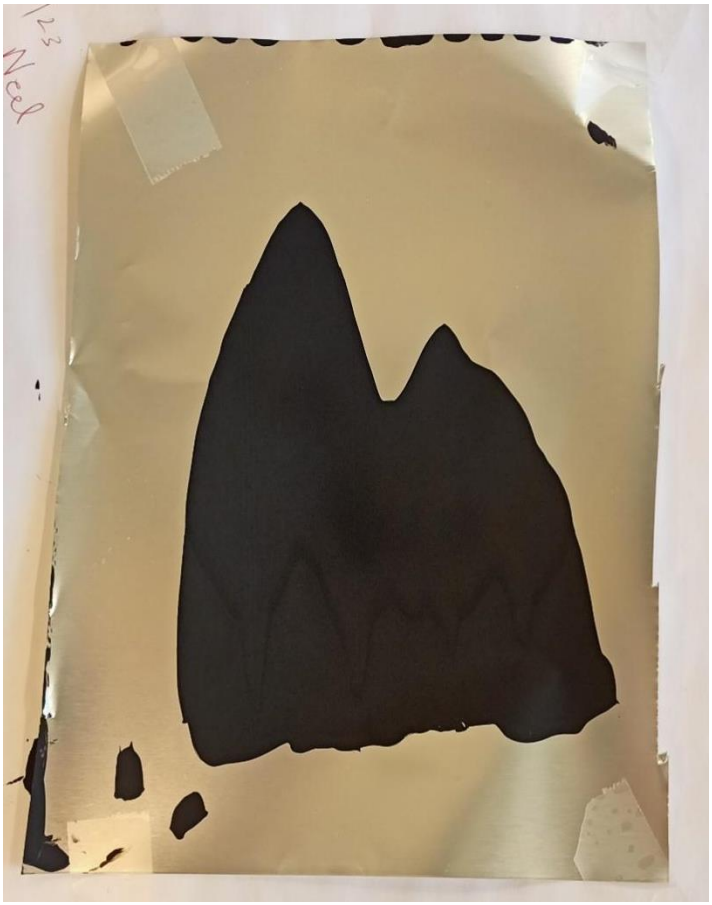

Figure 3.6: Aluminium foil with coated slurry for LFP cathode (before heating).

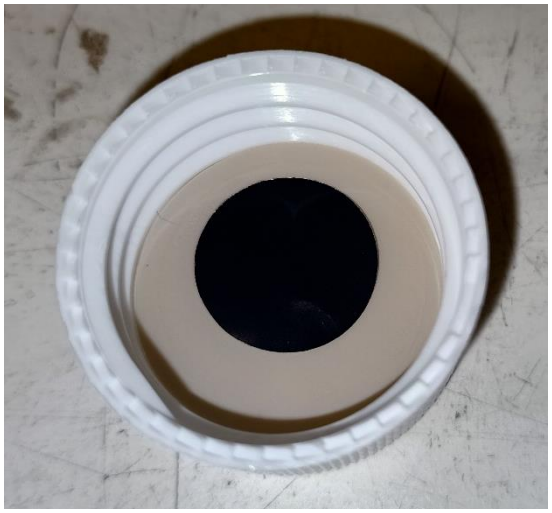

Figure 3.7: LFP cathode prepared by NMP based slurry method, Ø 13 mm.

3.2.2B Hybrid cathode preparation

Hybrid cathodes use both LFP and Li_4-PTtSA as active materials and aluminium foil is used as a cathode substrate. The hybrid cathode preparation is entirely done inside the glove box. A separate Kynar binder stock solution is prepared (80 mg per 1 ml NMP) using a magnetic stirrer (IKA RCT Basic). LFP and 50% of the C65 by weight are mixed using a pestle and mortar. Li_4-PTtSA and the remaining C65 are mixed separately. 500 microliters of the stock solution are added to the LFP - C65 mixture and mixed well. The Li_4-PTtSA – C65 mixture is added to the formed paste and this final mixture is ground with the gradual addition of 400 microliters of NMP. The formed slurry is put on a cleaned aluminium foil (rough side) and a 100-micron thick coating is made using a coater bar. Composition of the slurry used for coating can be found in **Table S2**, in Section 6.3 of the supplementary information. The ratio of the active material to C65, binder is 8:1:1 (by weight). The ratio of Li_4-PTtSA to LFP is 1:4 (by weight). This coating is allowed to dry for 2 hours, after which it is heated at 110 °C in a tube furnace (BÜCHI Glass oven B-585) for 20 hours. After this heating process, the coated foil is cut into circular electrodes of 11 mm diameter using a hand cutter, inside the glove box. Weighing paper is used during the cutting process to prevent any damage to the electrodes. These hybrid cathodes are always kept under an inert atmosphere.

Figure 3.8: Aluminium foil with coated slurry for hybrid cathode (before heating).

3.2.3 Cell assembly processes

All cell components except electrolyte salts/solvents were adequately vacuum dried at 70 °C before they were transferred to the glove box (MBraun MB200B). Electrolyte or individual salt/solvent bottles were transferred in a packed and sealed condition and were opened only inside the glove box. Lithium anodes used in the cells were hand polished inside the glove box before assembly and were cut into 13mm diameter circles in case of Li-Cu cells.

Copper current collectors used in anode free and lithium half cells were cut as circles of 19mm diameter from copper foil (15 micron thickness) and cleaned by shaking in 1M HCl for 5 minutes followed by repeated rinsing with water and ethanol (3 times each). It must be noted that the copper foil has a rough side which appears dull and has a linear surface texture and a smooth side, which appears bright. The rough side is used for electrochemical study. Celgard separators were cut as circles of 19 mm diameter from the available roll (Celgard 2325). Cell casings, springs and stainless steel current collectors were used without any pretreatment. SS316 cell casings of CR2032 type coin cells were used

The Li half cells, Li-Cu cells, powder cells and anode free cells were assembled inside the glove box. The assembly scheme for the cells is shown in **Figure 3.9**. The general method

was to start from the cathode (+) case and finish with the anode (-) case. After assembly the cell was pressed using a cell assembly machine (TOB MR-120) with a force of 700 kg.

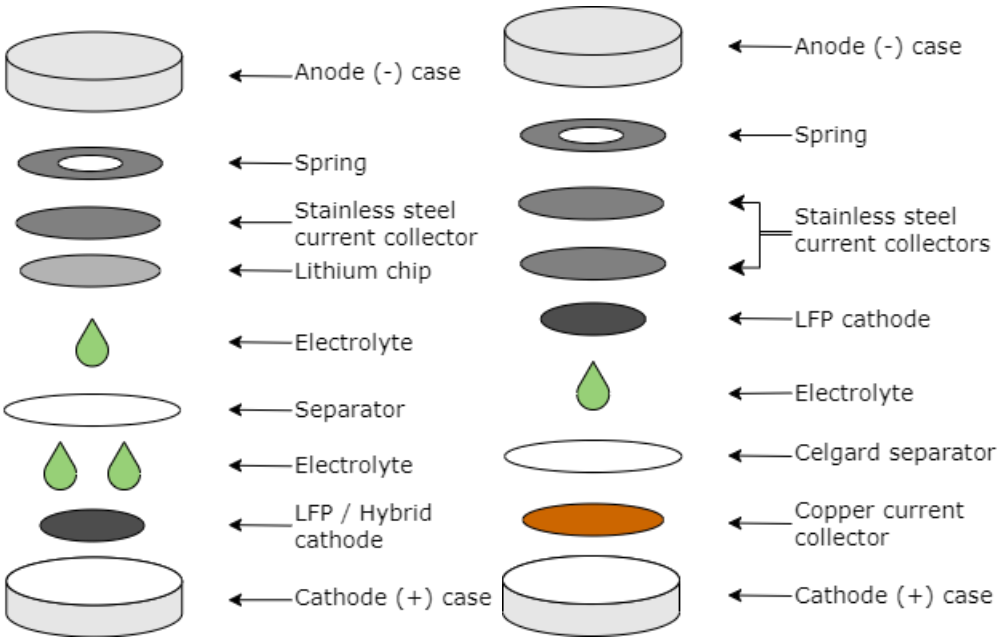

Figure 3.9 a: Assembly schemes for Li half cell (L) and anode free cell (R).

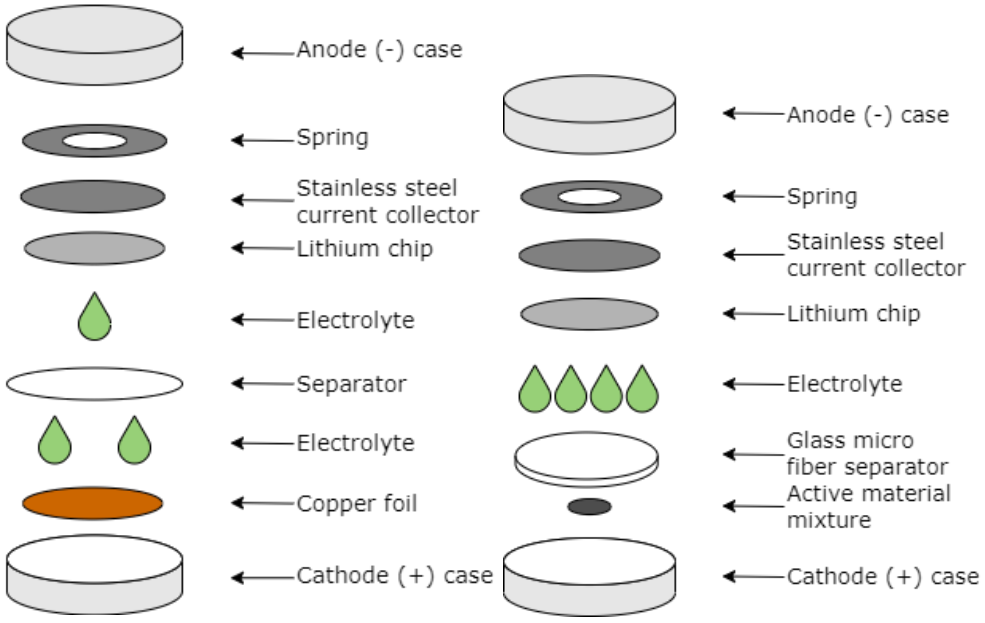

Figure 3.9 b: Assembly schemes for Li-Cu cell (L) and powder cell (R).

3.2.4 Galvanostatic cycling

Galvanostatic cycling (GC) is one of the most common methods applied to batteries for electrochemical characterization. It is primarily aimed at analysing and comparing the performance of a cell for different electrode/electrolyte systems for a given number of cycles. Essentially a selected value of current is applied to the cell until it is charged for a selected capacity (Capacity controlled cycling) or to a selected cut-off potential (Potential controlled cycling). Then the cell is discharged for a selected capacity or to a selected cut-off potential. The various variables involved like the time, current, potential, capacity and energy are recorded by the software. BioLogic BCS-05 with BT-Lab V1.60 software, and Neware battery testing system with BTS 7.6.0 software are used for recording the data. BTSDA 7.6.0 and OriginPro 2021b are used for data analysis.

An overview of galvanostatic cycling results for a LFP – Lithium half cell has been shown in **Figure 3.10**. The cell is cycled between cut-off potentials of 3.0 and 3.8 V. Variation of capacity with potential has been shown for the first cycle and variation of charge and discharge capacities has been shown for the first 150 cycles.

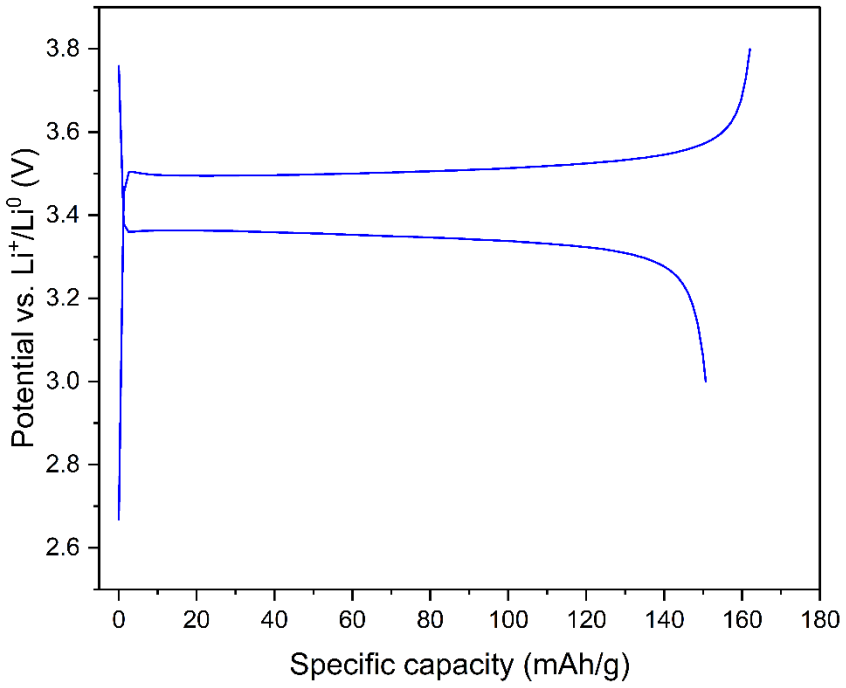

Figure 3.10 a. GCD pattern for first cycle.

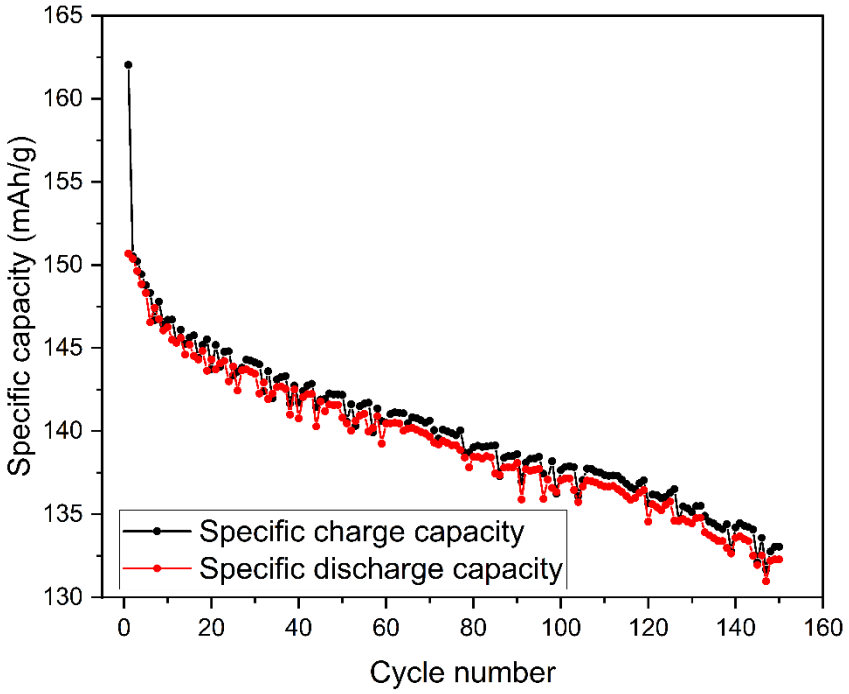

Figure 3.10 b. Specific charge and discharge capacities for 150 cycles.

Figure 3.10: GCD data for LF8P – lithium half cell: Current density of 0.2 mA/cm^2
Cathode/Anode: LFP electrode/Polished lithium chip
Electrolyte: 2M LiFSI + 1M LiTFSI in DOL/DME (1:1 v/v)

4 Experiments towards anode free battery optimization

4.1 Lithium copper cells: Observing the copper anode substrate

It has been clearly established that a net improvement in the long term performance of an anode free cell will be a result of two separate actions:

1. Improving the quality of the initially formed SEI at the anode substrate surface, to increase average coulombic efficiency by minimizing the active lithium lost at each cycle.
2. Forming an in-situ developed lithium reservoir on the anode substrate, to replenish active lithium lost at each cycle.

Towards this end, the copper anode substrate can be paired with lithium metal to form a reversible energy storage system (henceforth referred to as Li-Cu cell) which can help in understanding the nuances regarding improving the initial SEI formation and forming the in-situ developed lithium reservoir. It is important to note that although this system shows a reversible energy storage behaviour, it does not resemble a potential type of rechargeable battery. An exploded view of the Li-Cu cell structure has been shown in **Figure 4.1**.

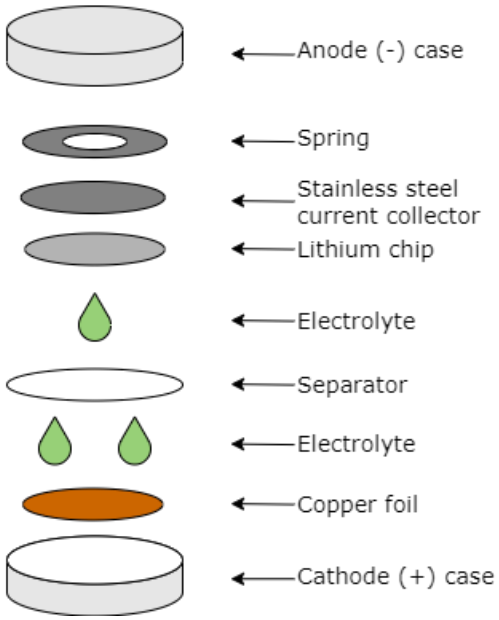

Figure 4.1: Exploded view of the Li-Cu cell structure.

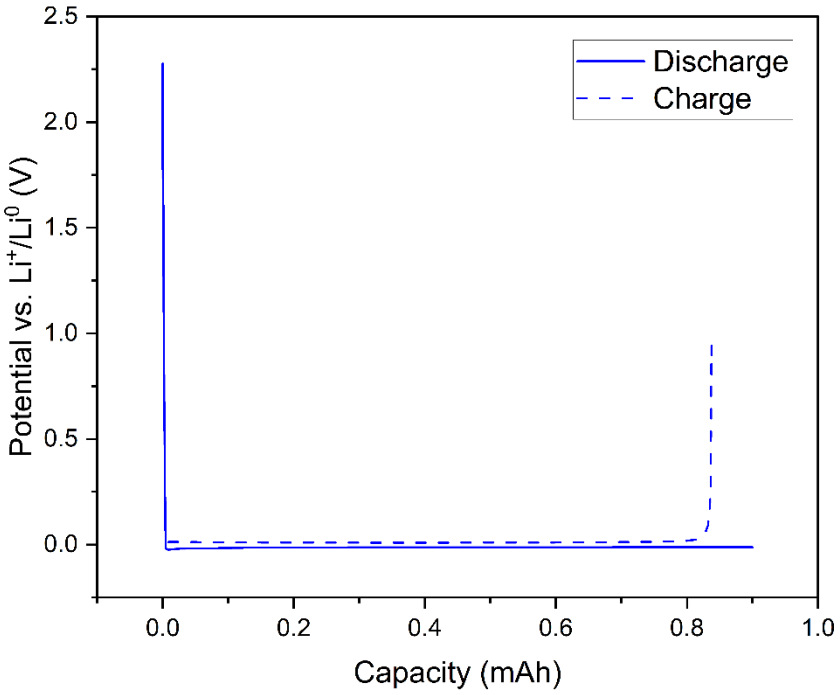

Figure 4.2 a: GCD pattern for first cycle.

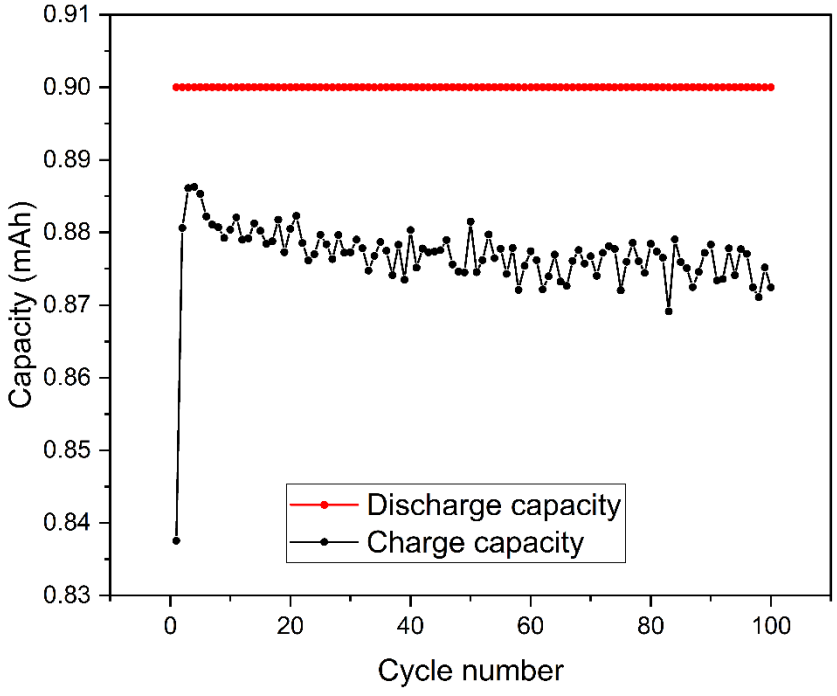

Figure 4.2 b: Charge and discharge capacities for 100 cycles.

GCD data for Li – Cu half cell: Current density of 0.2 mA/cm^2
Cathode/Anode: Copper foil/Polished lithium chip
Electrolyte: 2M LiFSI + 1M LiTFSI in DOL/DME (1:1 v/v)

As it can be seen in the **Figure 4.1**, the cathode (copper foil) is initially in a delithiated state which implies that the cell is assembled in a charged state. Hence the energy storage cycle consists of a discharge process followed by a charge process. The discharge process consists of deposition of a specified capacity of lithium metal on the copper foil (lithium electroplating), and the charge process consists of a specified capacity of lithium metal leaving the copper surface and returning to the lithium chip (lithium electrodissolution). Special attention must be paid to the fact that the GCD pattern for a Li-Cu cell appears very different than that for a Li half cell or anode free cell. GCD data for a Li half cell was shown in **Figure 3.10** on Page 39. In **Figure 4.2**, GCD data has been shown for the Li-Cu cell cycled with an uninterrupted first cycle (Cycling protocol given in **Table 4.1**, left part).

As it can be seen in **Figure 4.2 a**, The GCD pattern for a Li-Cu cell is substantially different for a Li-Cu cell from that for a Li half cell or anode free cell. For the specific cell involved, the OCV after cell assembly was approximately 2.25 V. As the cell is discharged, a certain mass of lithium corresponding to 0.9 mAh is electroplated onto the copper foil. When the cell is charged, theoretically the same amount (0.9 mAh) of lithium must strip from the copper foil and deposit back onto the lithium chip, but around 0.06 mAh worth of lithium is lost due to SEI formation and other inefficiencies. The difference between the discharge and charge capacities for 100 cycles has been shown in **Figure 4.2 b**.

It is also important to note that while a change in the specific capacity is normally used to quantify cell performance, this value cannot be calculated for a Li-Cu cell as no characteristic mass is associated with a particular Li-Cu cell. Hence capacity is used instead of specific capacity.

4.1.1 Application of the intermediate rest step

It is well understood that the long term performance of a rechargeable battery is heavily influenced by the formation of a stable and robust SEI. In order to understand the effects of improved SEI formation at the anode substrate surface, Li-Cu cells are cycled by two methods:

1. With an uninterrupted first cycle
2. With a 24 hour rest between the 1st discharge and 1st charge (Intermediate rest step), and the performance for the two cases is compared.

The main rationale behind having a 24 hour rest period after the 1st discharge is to give the system a certain amount of time with no electrical activity, to form a stable SEI on the copper foil after initial lithium deposition. This technique was highlighted in a past work [52] which investigated the effects of electrolyte concentration and resting protocol on the cycling stability of anode free batteries. The cycling protocols for cycling with an intermediate rest step and the control case (Uninterrupted first cycle) are given in **Table 4.1**.

Table 4.1: Cycling protocols for cycling with uninterrupted first cycle and cycling with an intermediate rest step for a Li-Cu cell.

	Uninterrupted first cycle (control case)					24-hour rest between 1st discharge and 1st charge (intermediate rest step)				
ID	Step name	Step time (hrs)	Volt (V)	Curr. (mA)	Cap. (mAh)	Step name	Step time (hrs)	Volt (V)	Curr. (mA)	Cap. (mAh)
1	Rest	4				Rest	4			
2	Discharge			0.265	0.9	Discharge			0.265	0.9
3	Charge		1	0.265	0.9	Rest	24			
4	Cycle	Begin ID: 2		Times: 99		Charge		1	0.265	0.9
5						Discharge			0.265	0.9
6						Charge		1	0.265	0.9
7						Cycle	Begin ID: 5		Times: 98	

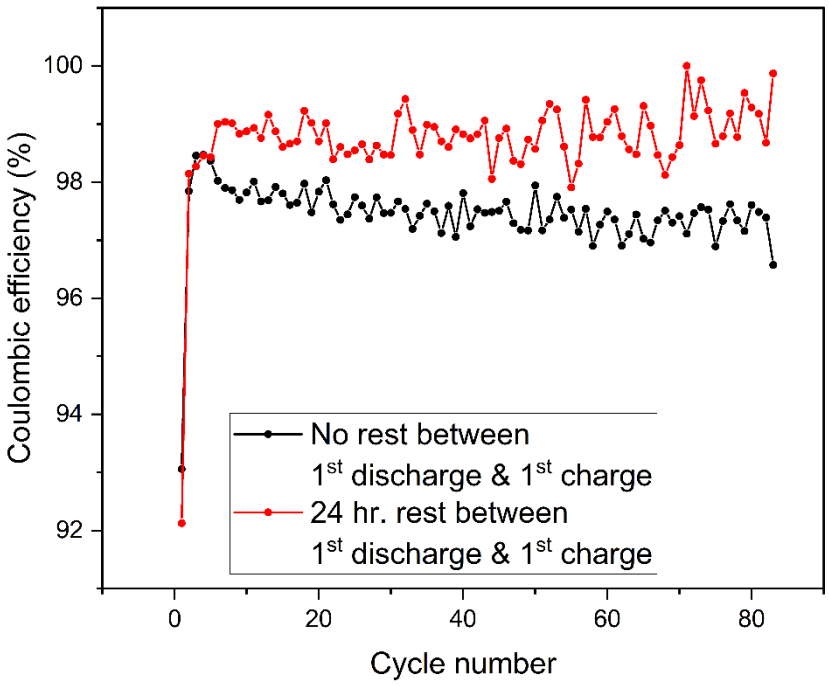

Figure 4.3: CE data for two cases, with and without the intermediate rest step.

The efficiency data for the two cases is shown in **Figure 4.3** and it is observed that on introduction of the intermediate rest step, the first cycle CE decreases by ca. 1 %, implying higher consumption of active consumption during initial SEI formation. But on the other hand, introduction of the intermediate rest step improves cell performance by a certain extent. While the 80 cycle average CE for the cell with no intermediate rest step is 97.5 %, with an intermediate rest step it is 98.7 %. This improvement may appear marginal but when one observes the data in **Table 4.2**, it can easily be understood that this increase in average CE will improve long term cell performance by a large extent.

Moreover, it can be shown that this increase in average CE from 97.5 % to 98.7 % improves the cycle life by more than 100 %. It is assumed that the cell reaches end of life when it can only charge up to 80 % of the initial charge capacity and 'n' cycles are completed before end of life is reached. It is well known that Coulombic efficiency for a given cycle is the ratio of discharge capacity to charge capacity. Considering this basic definition, the following equations can be written:

$$80 = 100\,(\tfrac{97.5}{100})^{n_1} \quad \text{(Equation 4.1)}$$

$$80 = 100\,(\tfrac{98.7}{100})^{n_2} \quad \text{(Equation 4.2)}$$

The solutions of these equations are $n_1 = 8.81$ and $n_2 = 17.05$.

The number of cycles completed before the cell reaches end of life are 8 and 17 in the absence and presence of the intermediate rest step. This means that the cycle life increases by more than a 100 % in the case of application of an intermediate rest step. Thus, it can be said that if this intermediate rest step strategy is applied to an anode free cell, it has the potential to increase the life of an anode free cell by forming an initial SEI that is more stable and robust as compared to an initial SEI formed without an intermediate rest step.

Table 4.2: Cycles completed with 80% capacity retention for selected average CE values.

Average coulombic efficiency (%)	Number of cycles completed as charge capacity decreases to 80 % of initial value
99.99	2232
99.98	1116
99.95	447
99.8	112
99.5	45
99	23

4.1.2 Use of limited cycling to build a lithium reservoir

As outlined in Chapter 2, one of the goals of this study is to understand the use of Li_4-PTtSA as a sacrificial agent in anode free batteries, which would form a lithium reservoir on the copper anode substrate. In order to understand the nuances of this approach, it is important to understand the effect of presence of a lithium reservoir on the long term cell performance. With this aim, Li-Cu cells are cycled in two modes:

1. Full (Standard) cycling mode
2. Limited cycling mode, and performance for the two cells is compared.

The details of lithium reservoir formation, by limited cycling and with the help of a 'sacrificial agent' have been shown in **Figure 4.4**. Full cycling is the cycling of a Li-Cu cell such that the specified values of the discharge and charge capacities for the cell are equal throughout the life of the cell. The realized discharge capacity value will be equal for every

cycle as the lithium chip behaves as an infinite source of lithium. The realized charge capacity value will decrease with every cycle as active lithium is lost due to SEI, dead lithium and dendrite formation. Hence it can be said that full cycling helps to understand the details of SEI formation on a copper surface and active lithium loss with every cycle. Limited cycling is the cycling of a Li-Cu cell such that in the second cycle, a lithium reservoir is formed in-situ on the copper foil. The realized discharge capacity value will be equal to the specified discharge capacity value for each cycle, with the lithium chip behaving as an infinite source of lithium. The realized charge capacity value will decrease with every cycle as in the case of full cycling, but this decrease will be lower on average. The reason for this is that the active lithium lost in every charge process will be compensated by lithium present in the reservoir, for a part of the cycle life. The cycling protocols for full and limited cycling have been shown in **Table 4.3**.

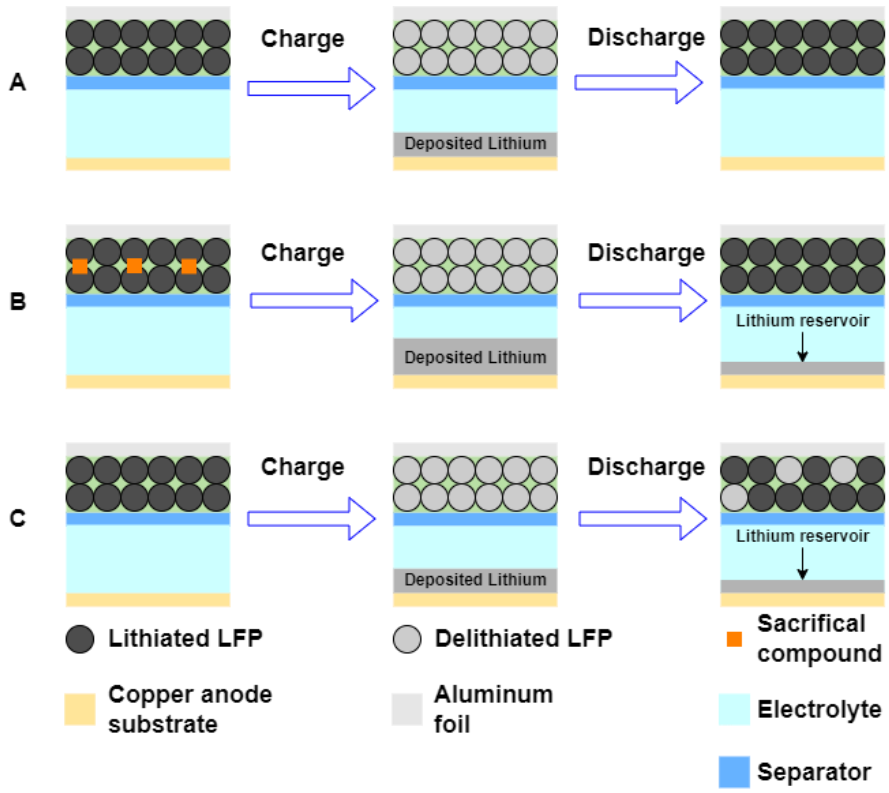

Figure 4.4: First cycle processes for three cases of anode free cells
A: Conventional anode free cell operation
B: Lithium reservoir formation by use of a sacrificial compound
C: Lithium reservoir formation by limited cycling

Since initial SEI formation is an important part of the ageing and the functioning of a cell, and a comparison can be made only when background factors are equal, both cells are allowed to form a full SEI with a 100 % initial discharge. In this way, 'SEI exclusion' is done to have an equal comparison. Thus, the first cycle for full and limited cycling comprises of a 100 % discharge and charge with a specified capacity of 0.9 mAh.

The next 99 cycles for full cycling also correspond to a 100 % discharge and charge with a specified capacity of 0.9 mAh. But the 2nd cycle for limited cycling involves a 100 % discharge and 80 % charge, which implies the creation of a lithium reservoir corresponding to 20 % of 0.9 mAh or 0.18 mAh. 3rd cycle onwards, limited cycling involves a discharge and charge with a specified capacity of 0.72 mAh (80 % of 0.9 mAh). In this way, a lithium reservoir is used to replenish the active lithium lost for a few cycles from the 3rd cycle onwards.

Table 4.3: Cycling protocols for full and limited cycling for a Li-Cu cell.

	Full cycling (100 %)					Limited cycling (80 %)				
ID	Step name	Step time (hrs)	Volt (V)	Curr. (mA)	Cap. (mAh)	Step name	Step time (hrs)	Volt (V)	Curr. (mA)	Cap. (mAh)
1	Rest	4				Rest	4			
2	Discharge			0.265	0.9	Discharge			0.265	0.9
3	Charge		1	0.265	0.9	Charge		1	0.265	0.9
4	Discharge			0.265	0.9	Discharge			0.265	0.9
5	Charge		1	0.265	0.9	Charge		1	0.265	0.72
6	Cycle	Begin ID: 4		Times: 98		Discharge			0.265	0.72
7						Charge		1	0.265	0.72
8						Cycle	Begin ID:6		Times: 97	

It has been clearly explained that the lithium reservoir is formed in the 2nd cycle and its capacity value is 0.18 mAh. A basic thumb rule says that 1 mAh of charge corresponds to 0.259 mg of deposited lithium, with 0.259 mg/cm^2 of lithium ideally being equivalent to a

4.82 µm thick layer [37]. Areal charge passed here is 0.136 mAh/cm^2, corresponding to an areal lithium deposition of 0.196 mg/cm^2 or a 3.65 µm thick layer of lithium.

Efficiency data for the two cycling modes has been shown in **Figure 4.5**. In case of limited cycling, it is observed that from the 3rd cycle onwards, the CE for a few cycles (11 to be precise) is 100 %. This is because the formed lithium reservoir replenishes the active lithium that is lost during cycling. Therefore, it can be said that in an anode free cell, a lithium reservoir (formed by use of a sacrificial agent or otherwise) has the potential to replenish the lost active lithium for a given number of cycles (11 cycles for 3.65 µm thick reservoir). This improves the long term capacity retention. When this concept is applied to an anode free cell (**Figure 4.9** on Page 55), there is an improvement in the average CE and the number of cycles completed for 70 % capacity retention increases by a large extent.

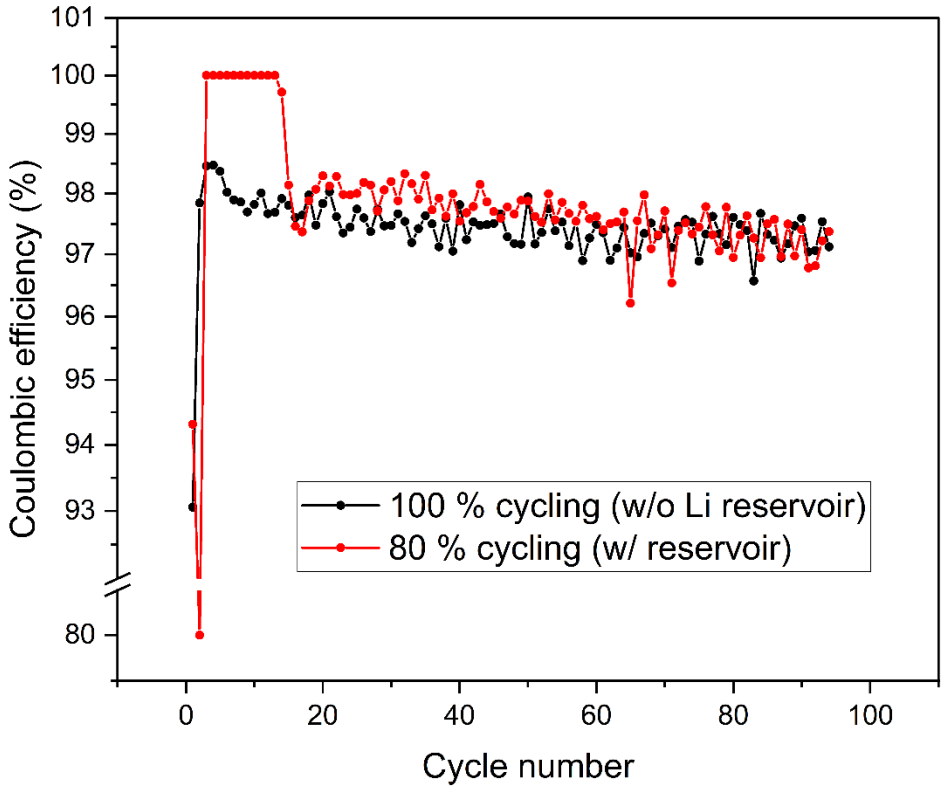

Figure 4.5: CE data for a Li-Cu cell with two cases, full and limited cycling.

4.2 Lithium half cells: Understanding the LFP cathode

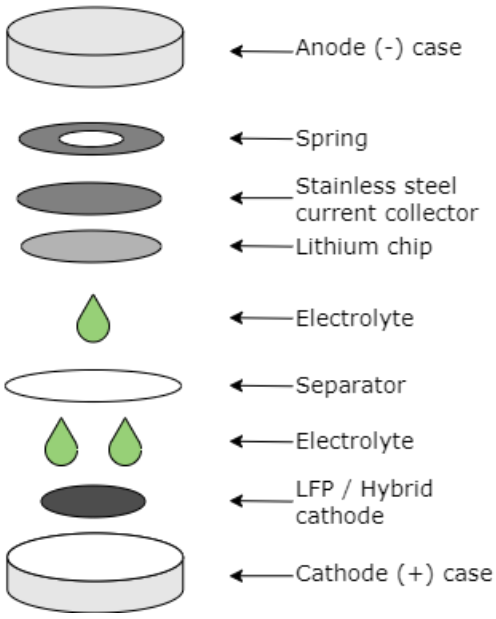

Figure 4.6: Exploded view of the Li half cell structure.

It is elementary knowledge for engineers and scientists specializing in batteries that in current lithium ion batteries, the cathode active material (CAM) contained in the cathode acts as the source of active lithium. As stated in Chapter 3, LFP is used as the CAM for this study. Currently used cathodes for lithium ion batteries consist of a solid aggregate supported on an aluminium substrate. At a laboratory level, the aggregate comprises of three materials: CAM particles (acting as lithium ion source and host), carbon based additive (to enhance electronic conductivity) and binder (responsible for structural integrity and adhesion with substrate). The cathode is prepared by a slurry based coating method where NMP is used as a solvent, the process has been outlined in Section 3.2.2.

On a broad level, the long term performance of a cathode is a function of two sets of parameters, compositional variables and process variables. Compositional variables include the CAM: carbon additive ratio and the CAM: binder ratio. Optimization is necessary here as a larger amount of carbon additive or binder decreases the areal capacity of the cathode. Also, LFP having a lower electronic conductivity [63], LFP cathodes require the use of an increased amount of carbon additive. Process variables include quality of slurry preparation, viscosity of slurry (controlled by amount of NMP used), pretreatment of substrate and quality of the coating process among others. In order to understand the working and performance of the

prepared cathode and the selected CAM, the cathode is paired with lithium metal to form a lithium metal system (henceforth referred to as Li half cell). This configuration resembles a lithium metal battery and the exploded view of the Li half cell structure has been shown in **Figure 4.6**.

One of the benchmark experiments involving Li half cells is to build a cell with an LFP cathode with cathode preparation as described in Section 3.2.2A. This allows us to observe the long term performance of the cathode and quality of the preparation process that is used. Performance data for the cell has been shown in **Figure 4.7** and **Table 4.4**.

With a discharge capacity loss of around 12% over 150 cycles and a 150 cycle average CE of 99.47 %, it can be said the efficiency wise, the performance is reasonable. But on the other hand, it can be clearly seen that the cathode suffers from a large increase in overpotential as number of completed cycles increases. This increase is termed as 'polarisation'. This is a disadvantage as polarisation results in the cell charging at a higher potential than expected and the cell discharging at a lower potential than expected. Other than characteristic polarisation expected from the cathode material, there are multiple other factors related to the cathode fabrication and battery chemistry which give rise to polarisation. A major contribution is due to delamination of the cathode coating from cathode substrate (aluminium current collector). Regarding the chosen electrolyte, the presence of a high concentration of LiFSI salt may have a corrosive effect on the aluminium surface, which may result in increased polarisation.

Also, the first cycle CE is only ca. 93%. The LFP, C65 and Kynar used were used directly from their containers and it is believed that this leads to water being present in the slurry. Drying the powders before use can possibly lead to an improvement in the first cycle CE and stability of the cathode.

Table 4.4: Performance data for LFP – Li half cell.

Cycle no.	CE (%)	Relative discharge capacity	Approximate polarization (mV)
1	92.98	1	140
30	99.53	0.952	180
60	99.97	0.932	200
90	99.61	0.916	230
120	99.19	0.893	240
150	99.41	0.878	300

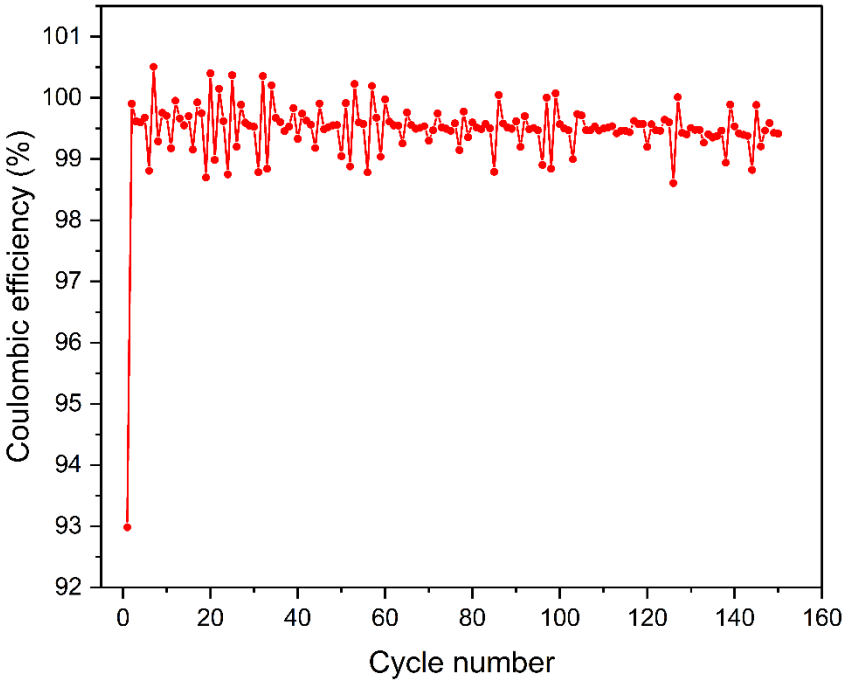

Figure 4.7 a: Efficiency data for 150 cycles.

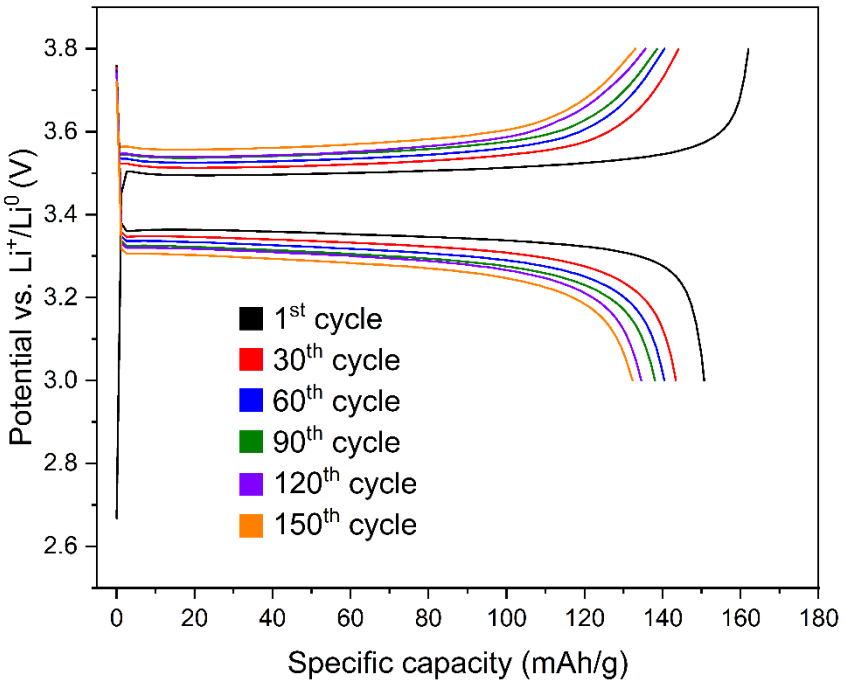

Figure 4.7 b: Capacity – Potential data for 150 cycles.

Figure 4.7: GCD data for LFP – lithium half cell: Current density of 0.2 mA/cm^2
Cathode/Anode: LFP electrode/Polished lithium chip
Electrolyte: 2M LiFSI + 1M LiTFSI in DOL/DME (1:1 v/v)

4.3 Anode free cells: Brief experiments

In order to understand the behaviour of an anode free cell, an LFP cathode is paired with a copper anode substrate and the resulting configuration resembles a typical anode free battery. It can be said that the net inefficiency for this system is a result of the inefficiency of intercalation/deintercalation at the coated cathode and inefficiency of lithium electroplating/ electrodissolution at the copper anode substrate. Exploded view of the anode free cell structure has been shown in **Figure 4.8**.

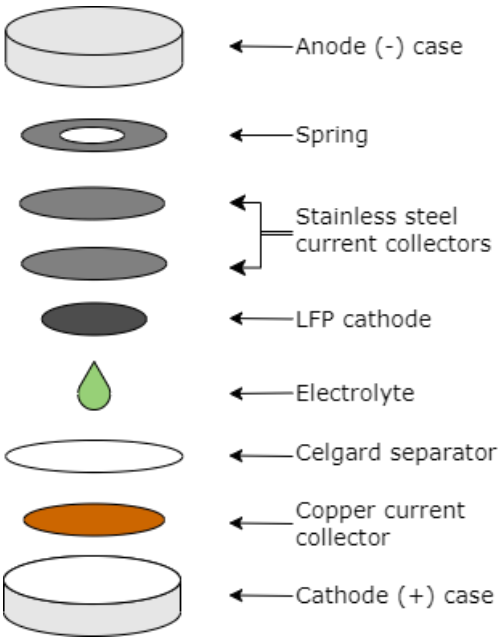

Figure 4.8: Exploded view of the structure of an anode free cell

With regards to nuances in construction, two stainless steel current collectors are used instead of one to accommodate for the lost thickness as here the cathode (LFP electrode) and anode substrate (copper foil) both are foils and have thicknesses in the micrometre domain.

In order to understand the effect of lithium reservoir formation on anode free cell performance, behaviour for full and limited cycling are compared with each other. Full cycling consists of varying the cell potential between 3.0 and 3.8 V at a constant current density of 0.2 mA/cm^2. In this case the entire available capacity of the cathode is utilised for all cycles. Limited cycling uses a 70 % discharge step in the second cycle to build a lithium reservoir on the copper anode substrate which is equal to 30% of the initial cathode capacity. The cycling protocols for the full and limited cycling have been shown in **Table 4.5**.

Table 4.5: Cycling protocols for full (standard) and limited cycling for an anode free cell.

	Full (Standard cycling) (100 %)					Limited cycling (70 %)				
ID	Step name	Step time (hrs)	Volt (V)	Curr. (mA)	Cap. (mAh)	Step name	Step time (hrs)	Volt (V)	Curr. (mA)	Cap. (mAh)
1	Rest	4				Rest	4			
2	Charge		3.8	0.265		Charge		3.8	0.265	
3	Discharge		3.0	0.265		Discharge		3.0	0.265	
4		Begin ID: 2		Times: 99		Charge		3.8	0.265	
5						Discharge		3.0	0.265	0.487
6						Charge		3.8	0.265	0.487
7						Discharge		3.0	0.265	0.487
8						Cycle	Begin ID:6		Times: 97	

Table 4.6: Limited cycling capacity data for 4 initial cycles.

Cycle	Capacity (mAh)		Coulombic efficiency (%)
1	Charge	0.71625	77.52
	Discharge	0.55522	
2	Charge	0.55993	87.02
	Discharge	0.48723	
3	Charge	0.48726	99.99
	Discharge	0.48722	
4	Charge	0.48722	100.00
	Discharge	0.48722	

A detailed analysis of the .nda file for limited cycling as shown in **Table. 4.6** shows that capacity of the lithium reservoir in the second cycle formed is 0.0727 mAh, and thus the thickness of the lithium reservoir is ca. 0.26 µm. In an ideal case, the reservoir capacity should have been nearly equal to 30% (ca. 0.29 mAh) of the initial cathode capacity (0.696 mAh calculated, 0.716 mAh observed). But due to high lithium consumption in the first cycle due to low first cycle CE, 0.161 mAh worth of lithium was lost in SEI formation. As a result,

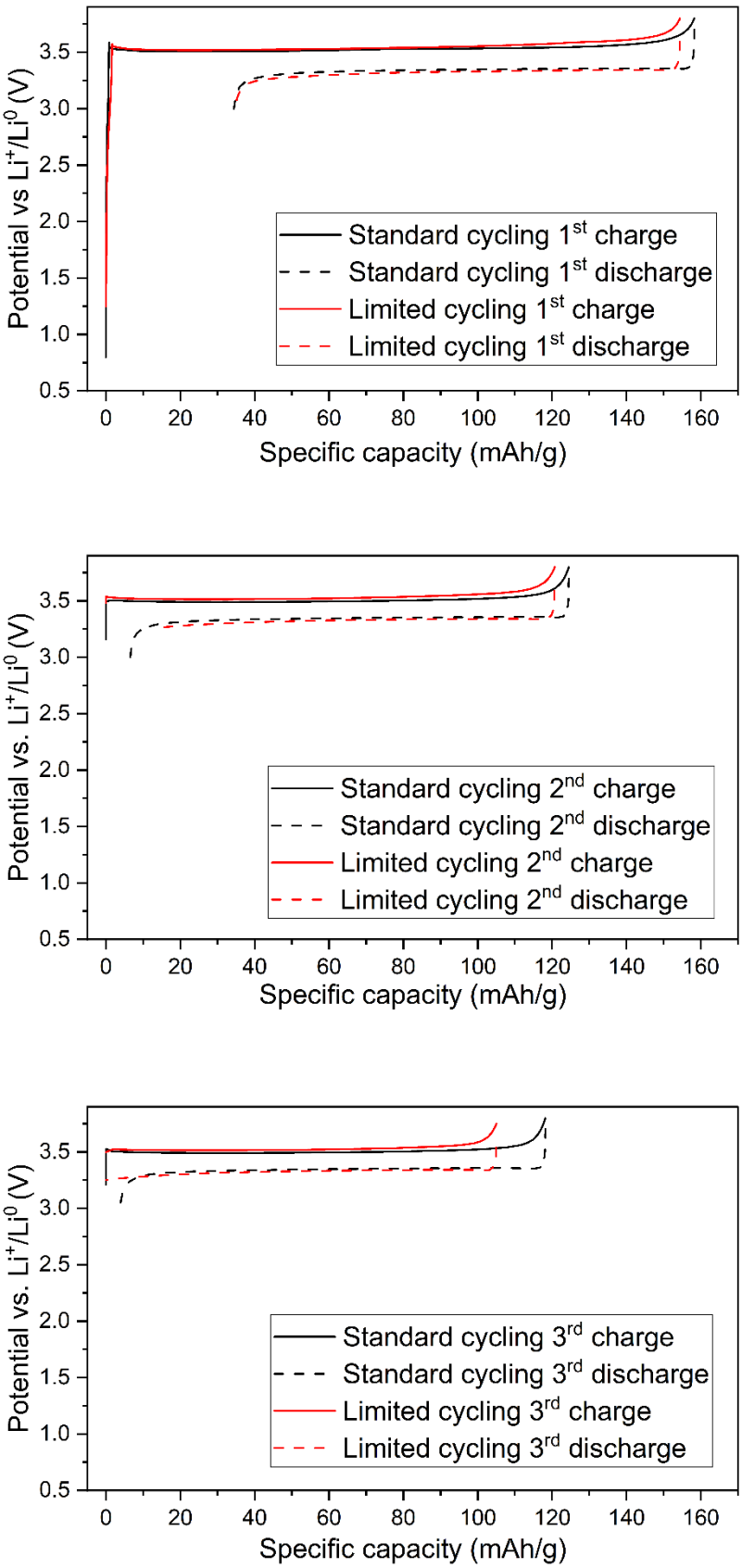

Figure 4.9 a: Butterfly plots for first 3 cycles of anode free cells with full and limited cycling.

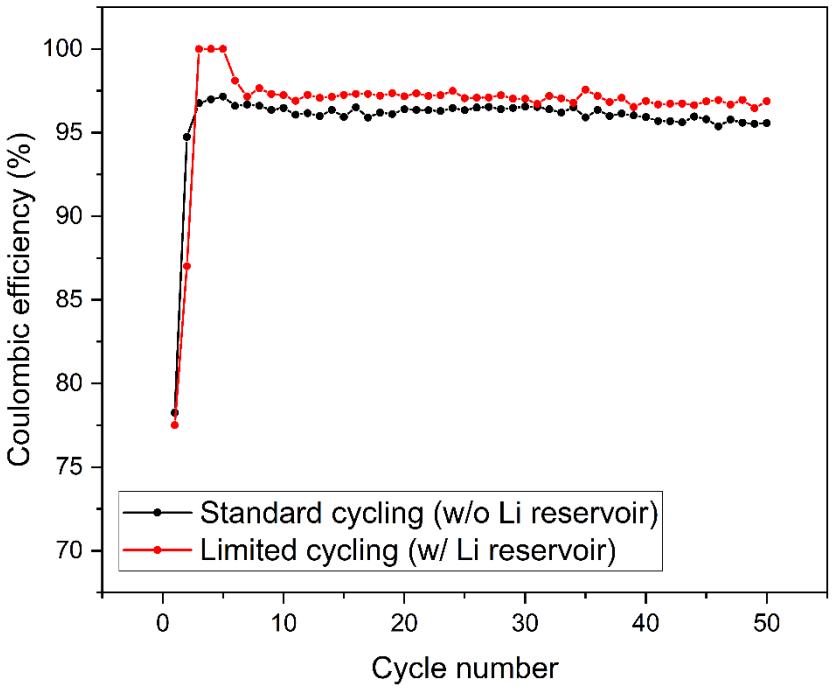

Figure 4.9 b: Efficiency data for 50 cycles.

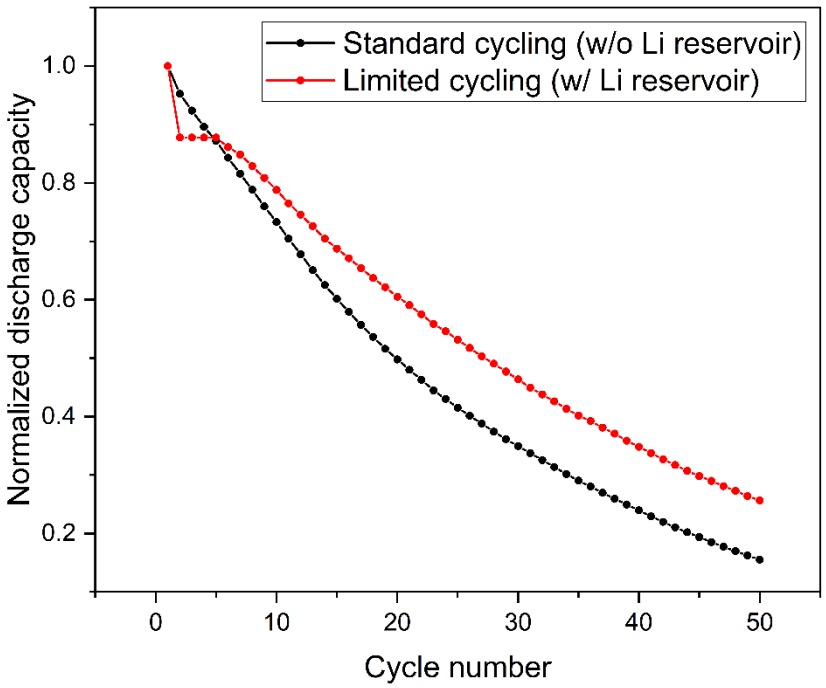

Figure 4.9 c: Discharge capacity data for 50 cycles.
Figure 4.9: GCD data for anode free cell with full and limited cycling
Current density of 0.2 mA/cm^2
Cathode/Anode: LFP electrode/Copper foil
Electrolyte: 2M LiFSI + 1M LiTFSI in DOL/DME (1:1 v/v)

the reservoir contained only 0.0727 mAh worth of lithium. The CE was found to be 87 % instead of 70 % as the charge capacity for the second cycle was lower than what it was supposed to be.

$$Coulombic\ efficiency = \frac{Discharge\ capacity}{Charge\ capacity} \times 100\ \% \quad \text{(Equation 4.3)}$$

It can be said that as of now the low first cycle CE does not allow to implement a proper limited cycling protocol for lithium reservoir formation. The first cycle CE for anode free cells for standard and limited cycling is 78(±0.5) % (as shown in **Figure 4.9 a**). Such a high inefficiency again points towards the need for a detailed study about SEI structure and SEI formation processes, with optimization of first cycle conditions to form a high quality SEI with low active lithium loss. One could argue that the low first cycle CE could be offset by increasing ideal reservoir capacity from 30 % to 50 %. But as this percentage increases, the normal cycling capacity of the cell decreases (70 % to 50 %) which leads to inefficient use of the cathode in the long term.

On the other hand, lithium reservoir formation does improve the cycle life to a certain extent. The formed reservoir replenishes the lost active lithium for cycles 4 & 5, and therefore CE for these cycles is 100% (**Refer Figure 4.9 b**). In fact, even for cycle 3 with limited cycling the CE is 99.99 % while for standard cycling it is only 96.77 % (Refer **Figure 4.9 a**). It can be seen in **Figure 4.9 c** that this replenishment increases the number of cycles it takes for the cell to lose a given fraction of its initial discharge capacity. For instance, the anode free cell without a lithium reservoir loses half of its initial discharge capacity in 20 cycles, while the one with a lithium reservoir does so in 28 cycles. This corresponds to a cycle life increase of 40%. This increase is observed with a lithium reservoir that is capacity wise much smaller than the targeted capacity.

On a broad level, it can be said that if the lithium reservoir would have been constructed by oxidation of Li_4-PTtSA acting as a sacrificial agent, the lithium layer formed would have given a similar improvement in cycle life given that the lithium reservoir had an equal mass.

4.4 LFP – Li_4-PTtSA mixtures: Wet coated & Dry powder electrodes

As stated in Chapter 2, one of the aims of this study is to investigate the feasibility of Li_4-PTtSA for use in anode free batteries as a sacrificial agent for lithium reservoir formation. This organic compound will be contained in the cathode, thus calling for a hybrid cathode which contains two active materials. Thus it is also important to observe the joint behaviour of LFP and Li_4-PTtSA as a mixture. Powder cells are used for this purpose. A powder cell uses a substrate-less cathode consisting of the active material mixture in powder form paired with lithium metal as the anode. The exploded view of the powder cell has been shown in **Figure 4.10**. A glass microfiber separator is used in a powder cell instead of a Celgard separator.

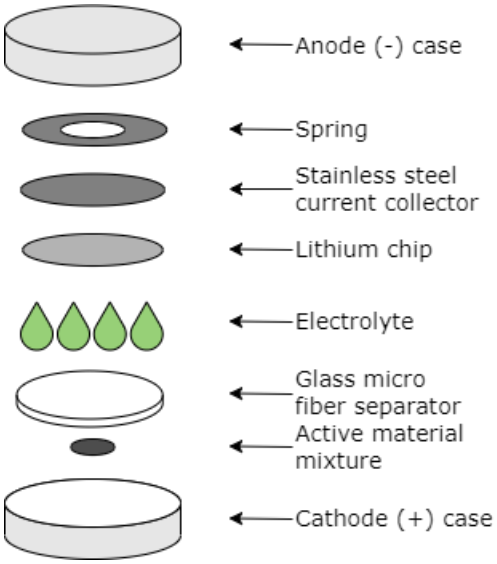

Figure 4.10: Exploded view of a powder cell.

.

4.4.1 Dry powder electrode

It is well established that LFP releases/accepts Li^+ ions by deintercalation/intercalation while and Li_4-PTtSA does by a standard oxidation/reduction process. It is important to understand the nuances of these processes when both these materials are used together as active materials. For a basic understanding, a powder cell is used with an active material mixture where the ratio of the constituents is the same as it will be in the hybrid cathode. Ratio of LFP to Li_4-PTtSA by mass is 4:1. The GCD pattern for the first two cycles has been shown for the first

two cycles in **Figure 4.11**. It can be clearly seen that both the active materials show a near-constant potential lithium ion release/absorption. And although the first Li_4-PTtSA oxidation process involves a ~120 mV overpotential, the oxidation still occurs outside the 3.0-3.8 V window. The GCD data for a powder cell consisting of an LFP - Li_4-PTtSA mixture thus allows us to get a basic idea about the joint behaviour of the two active materials.

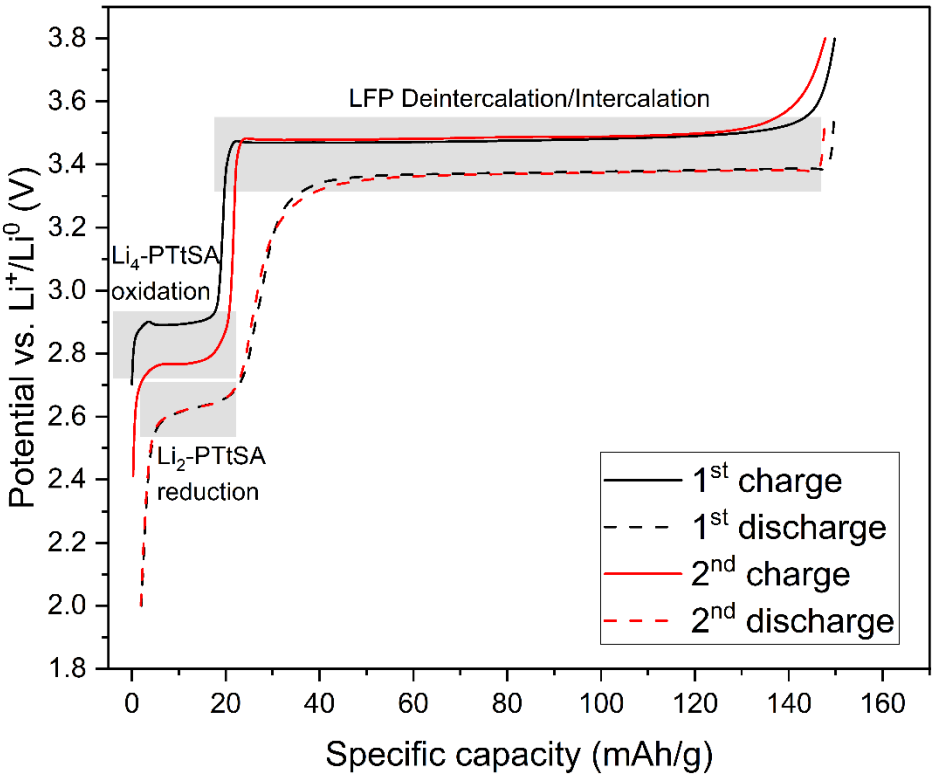

Figure 4.11: GCD data for powder cell: Current rate = C/10
Cathode/Anode: AM:C65:PVDF = 8:1:1 powder/Polished lithium chip
Electrolyte: 2M LiFSI + 1M LiTFSI in DOL/DME (1:1 v/v)

4.4.2 Wet coated electrode

To understand the joint behaviour of an LFP - Li_4-PTtSA mixture in a wet coated electrode (typical cell cathode), a wet coated electrode is prepared with coating thickness equal to 100 microns. This cathode is prepared inside the glove box and it is never exposed to ambient air. The preparation process has been explained in section 3.2.2B. The prepared cathode is used to assemble a lithium half cell and GCD data is observed. The GCD data for first 3 cycles for this cell has been given in Section 6.2 of the supplementary information.

The joint behaviour observed in case of a wet coated electrode is very different from the case of a dry powder electrode, despite the same LFP: Li_4-PTtSA ratio. In case of a wet coated electrode, Li_4-PTtSA oxidation does not occur over a near constant potential vs Li^+/Li^0. In order to understand the differences, the 1st cycle for both electrodes is compared. The relevant GCD data is shown in **Figure 4.12**.

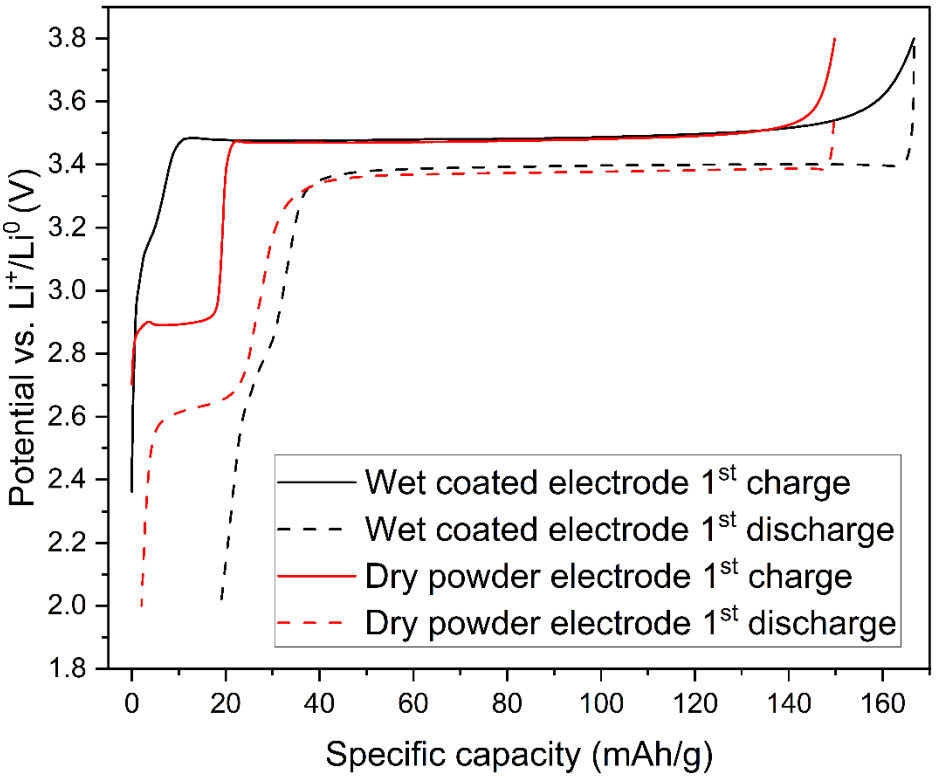

Figure 4.12: First cycle GCD data for coated (hybrid) electrode and powder cell. Active material for both cases is LFP: Li_4-PTtSA = 4:1

In case of a dry powder electrode, Li_4-PTtSA redox processes can be clearly identified whereas in a wet coated electrode these processes are not distinctly visible. This observation is attributed to the interaction of Li_4-PTtSA with NMP as the cathode coating and handling is done in an inert atmosphere inside the glove box and the electrode is never exposed to ambient air. Possible reactions of Li_4-PTtSA with NMP are not completely understood at this point of time. It is suspected that NMP partially dissolves Li_4-PTtSA with possible phase separation. At this point of time, it can be said that the given fabrication process for Li_4-PTtSA containing wet coated electrodes is sub-optimal and requires a substantial degree of improvement for production of cathodes capable of showing the required behaviour.

5 Conclusion and Perspectives

On a broad level it can be said that multiple battery systems exist which can be a potential replacement for lithium ion batteries. An anode free battery is one such alternative to the lack of low cost high specific energy batteries. But at present, copious research and optimization are required before anode free batteries can be implemented as a viable product. Multiple optimization strategies have been tested so far for improving the coulombic efficiency (CE) of anode free batteries. This work primarily focused on optimization using Li_4-PTtSA as a sacrificial agent to develop a lithium reservoir on the anode substrate to improve the cycle life of the cell.

Application of an intermediate rest step in the first cycle resulted in an increase in the long-term average CE of a lithium copper system. This improvement stems from an increase in the initial SEI stability due to the rest period available after the initial lithium deposition on the copper surface. As a result of this modification, the long term coulombic efficiency improved from 97.5 % to 98.8 %, which translates to a more than 100 % increase in cycle life. This concept can be carried over to an anode free system to improve long term performance.

Li_4-PTtSA was examined for use as a sacrificial agent for lithium reservoir development for anode free battery optimization. The sacrificial agent generates lithium ions which form a lithium reservoir on the anode substrate. As per the concept the lithium reservoir replenishes the active lithium lost during the initial cycles and directly results in an increase in the cycle life. Li_4-PTtSA containing hybrid cathodes were successfully fabricated in an inert atmosphere, but it was observed that NMP partially dissolves Li_4-PTtSA with possible phase separation. The fabrication process requires a substantial improvement. The lithium reservoir is also built without the use of a sacrificial agent by making use of limited cycling. With this process, an increase of 40% in the cell life is realised in an anode free cell for the considered case.

Speaking about the next steps that can be taken towards anode free battery optimization by building a lithium reservoir with a sacrificial agent, four things can be done in the short term. The first step is to develop a mathematical relationship between the mass of the lithium

reservoir and the increase in the cycle life of the cell. This will help to estimate the amount of Li_4-PTtSA required per cm^2 which must be present in the hybrid cathode (The oxidation efficiency of Li_4-PTtSA embedded in the hybrid cathode will also have to be established). After that, exhaustive studies will be required to analyse the effect of NMP on the Li_4-PTtSA molecule. If needed, a different solvent may have to be selected.

And keeping in mind that Li_4-PTtSA and LFP molecules are very different in terms of size, geometry and the chemical bonds involved (Both materials have different solubility properties as well), it will be intriguing to look at SEM/ TEM studies for the hybrid cathode in the lithiated/delithiated states before and after Li_4-PTtSA oxidation. Since the hybrid cathode will contain Li_2-PTtSA for the remaining life of the cell, it is important to work with electrochemical impedance spectroscopy or other in-situ studies to understand its behaviour on the performance of the cell.

In the long term, an important aspect of hybrid cathode development will be to increase the cathode coating thickness from 0.33 mAh/cm^2 LFP equivalent (100 micron) to 3 mAh/cm^2 LFP equivalent or higher. This is because commercial battery cathodes tend to have a minimum mass loading of 3 mAh/cm^2. Regarding lithium reservoir formation, optimization must be done for the first cycle charge and discharge current densities for better lithium reservoir integrity and adhesion to the copper anode substrate.

6 Supplementary information

6.1 Energy storage (redox) behaviour of Li_4-PTtSA

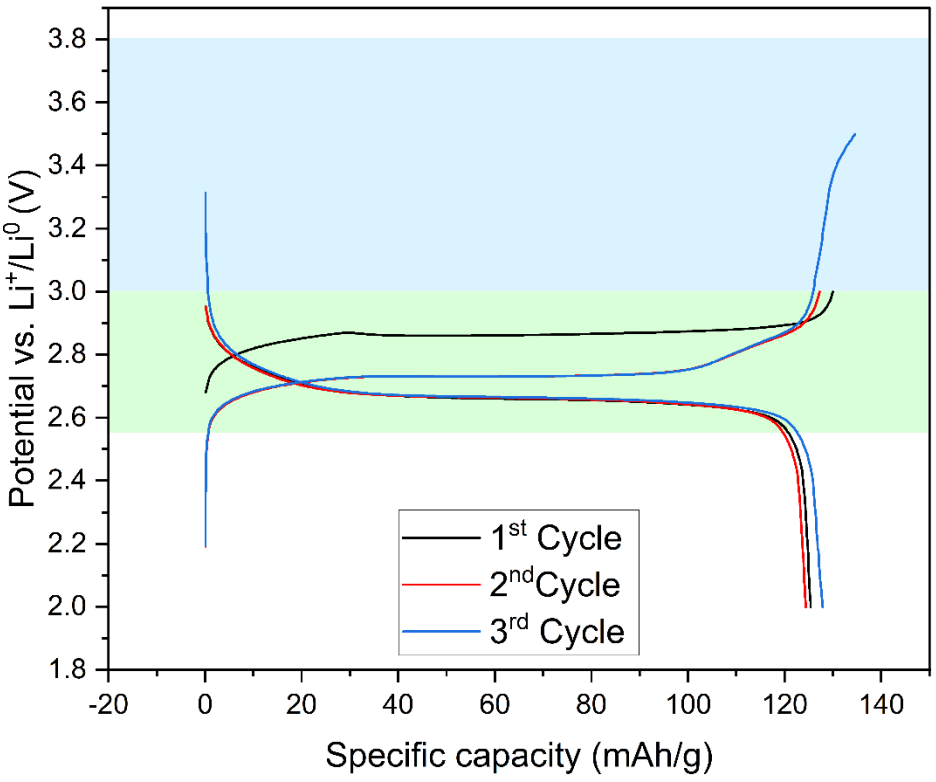

Figure S1: GCD data for powder cell at current rate = C/10
Cathode/Anode: = Li_4-PTtSA:SP = 2:1 powder/Polished lithium chip
Electrolyte: 2M LiFSI + 1M LiTFSI in DOL/DME (1:1 v/v)

A powder cell with Super-P carbon additive was used to verify the quality of Li_4-PTtSA that was prepared in-house. Synthesis of Li_4-PTtSA was done in accordance with the procedure as explained in prior research about the compound [62]. From the GCD data for 3 cycles, it can be clearly seen that the redox processes for Li_4-PTtSA are broadly confined to a potential region (green band) that is outside the standard LFP cell operation potential window of 3.0 – 3.8 V vs Li^+/Li^0 (blue band). This implies that Li_4-PTtSA can be oxidised to generate lithium ions (which would build a lithium reservoir on the copper anode substrate) in the first cycle itself before the potential reaches 3.0 V. More importantly, the cycling of the cell between 3.0 – 3.8 V will not involve any redox process concerning Li_4-PTtSA. Performance wise, the specific

capacity obtained is 120 mAh/g minimum, where the standard oxidation potential is ca. 2.75 V vs Li^+/Li^0. The oxidation potential for the first cycle is higher at ca. 2.85 V vs Li^+/Li^0. This is because Li_4-PTtSA in pristine (as prepared) case is poorly crystalline while at the end of the first charge Li_4-PTtSA appears to convert to a crystalline phase, as verified with in situ PXRD measurements [62].

6.2 Galvanostatic cycling behaviour for wet coated electrode with active material composition LFP: Li_4-PTtSA = 4:1

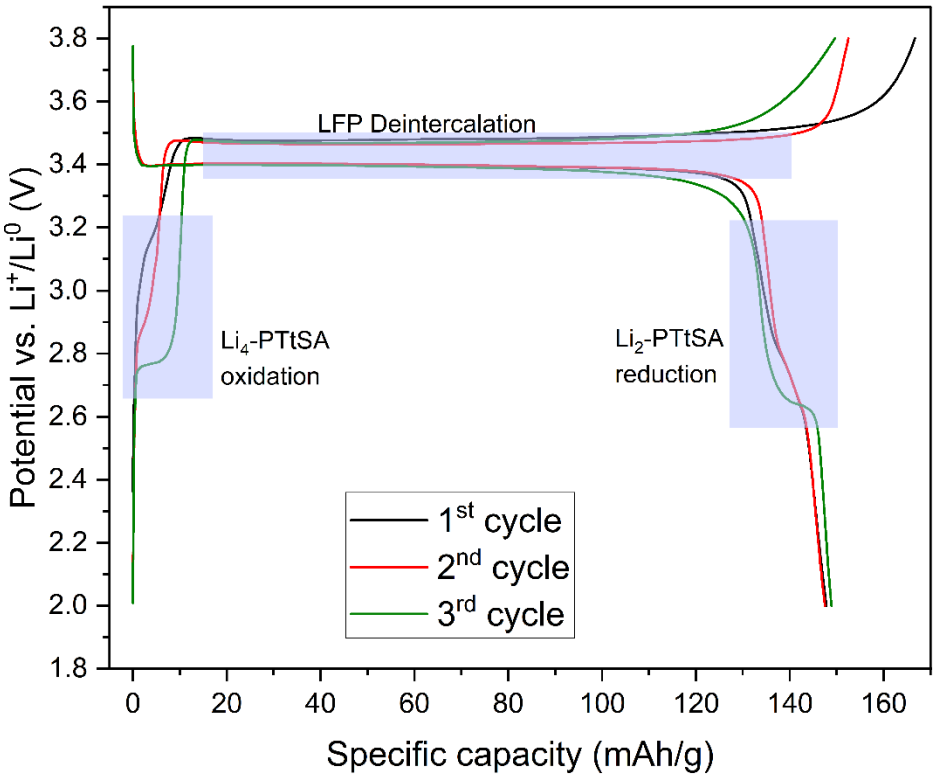

Figure 4.10: GCD data for wet coated electrode – lithium half cell
Current density of 0.2 mA/cm^2
Cathode/Anode: 100 micron wet coated electrode/Polished lithium chip
Coating composition: AM:PVDF:C65 = 8:1:1
Electrolyte: 2M LiFSI + 1M LiTFSI in DOL/DME (1:1 v/v)

For a wet coated electrode with active materials LFP & Li_4-PTtSA in the ratio 4:1, it observed that the redox behaviour of Li_4-PTtSA deviates from the behaviour observed for a dry powder electrode. The cause of this unwanted behaviour is attributed to the interaction of

Li_4-PTtSA with NMP as the cathode coating and handling is done in an inert atmosphere inside the glove box and the electrode is never exposed to ambient air. Possible reactions of Li_4-PTtSA with NMP are not completely understood at this point of time. It is suspected that NMP partially dissolves Li_4-PTtSA with possible phase separation.

6.3 Slurry composition for wet coated cathode preparation

Table S1: Composition of slurry used for LFP cathode preparation

No.	Material	Amount
1	LFP	160 mg
2	PVDF	20 mg
3	C65	20 mg
4	NMP	300 microliters

Table S2: Composition* of slurry used for hybrid cathode preparation

No.	Material	Amount
1	Li_4-PTtSA	64 mg
2	LFP	256 mg
3	C65	40 mg
4	Stock solution (80mg PVDF per 1ml NMP)	500 microliters
5	NMP	ca. 400 microliters

*This composition is only indicative as the viscous nature of the stock solution causes air bubbles to enter the micropipette when the volume of stock solution is being measured.

References

(1) Zwicker, M. F. R.; Moghadam, M.; Zhang, W.; Nielsen, C. V. Automotive Battery Pack Manufacturing – a Review of Battery to Tab Joining. *J. Adv. Join. Process.* **2020**, *1*, 100017. https://doi.org/10.1016/j.jajp.2020.100017.

(2) Zhao, G.; Wang, X.; Negnevitsky, M. Connecting Battery Technologies for Electric Vehicles from Battery Materials to Management. *iScience* **2022**, *25* (2), 103744. https://doi.org/10.1016/j.isci.2022.103744.

(3) Deng, J.; Bae, C.; Denlinger, A.; Miller, T. Electric Vehicles Batteries: Requirements and Challenges. *Joule* **2020**, *4* (3), 511–515. https://doi.org/10.1016/j.joule.2020.01.013.

(4) Zubi, G.; Dufo-López, R.; Carvalho, M.; Pasaoglu, G. The Lithium-Ion Battery: State of the Art and Future Perspectives. *Renew. Sustain. Energy Rev.* **2018**, *89*, 292–308. https://doi.org/10.1016/j.rser.2018.03.002.

(5) Muralidharan, N.; Self, E. C.; Dixit, M.; Du, Z.; Essehli, R.; Amin, R.; Nanda, J.; Belharouak, I. Next-Generation Cobalt-Free Cathodes – A Prospective Solution to the Battery Industry's Cobalt Problem. *Adv. Energy Mater.* **2022**, *12* (9), 2103050. https://doi.org/10.1002/aenm.202103050.

(6) Yang, G.; Abraham, C.; Ma, Y.; Lee, M.; Helfrick, E.; Oh, D.; Lee, D. Advances in Materials Design for All-Solid-State Batteries: From Bulk to Thin Films. *Appl. Sci.* **2020**, *10* (14), 4727. https://doi.org/10.3390/app10144727.

(7) Sun, P.; Bisschop, R.; Niu, H.; Huang, X. A Review of Battery Fires in Electric Vehicles. *Fire Technol.* **2020**, *56* (4), 1361–1410. https://doi.org/10.1007/s10694-019-00944-3.

(8) Chen, Y.; Kang, Y.; Zhao, Y.; Wang, L.; Liu, J.; Li, Y.; Liang, Z.; He, X.; Li, X.; Tavajohi, N.; Li, B. A Review of Lithium-Ion Battery Safety Concerns: The Issues, Strategies, and Testing Standards. *J. Energy Chem.* **2021**, *59*, 83–99. https://doi.org/10.1016/j.jechem.2020.10.017.

(9) Xu, K. A Long Journey of Lithium: From the Big Bang to Our Smartphones. *ENERGY Environ. Mater.* **2019**, *2* (4), 229–233. https://doi.org/10.1002/eem2.12057.

(10) Ramasubramanian, B.; Sundarrajan, S.; Chellappan, V.; Reddy, M. V.; Ramakrishna, S.; Zaghib, K. Recent Development in Carbon-LiFePO4 Cathodes for Lithium-Ion Batteries: A Mini Review. *Batteries* **2022**, *8* (10), 133. https://doi.org/10.3390/batteries8100133.

(11) Cao, W.; Zhang, J.; Li, H. Batteries with High Theoretical Energy Densities. *Energy Storage Mater.* **2020**, *26*, 46–55. https://doi.org/10.1016/j.ensm.2019.12.024.

(12) F., J.; Hasan, M.; Patil, S.; P., D.; Clancy, T. Energy Storage: Battery Materials and Architectures at the Nanoscale. In *ICT - Energy - Concepts Towards Zero - Power Information and Communication Technology*; Fagas, G., Ed.; InTech, 2014. https://doi.org/10.5772/57139.

(13) Choi, J. W.; Aurbach, D. Promise and Reality of Post-Lithium-Ion Batteries with High Energy Densities. *Nat. Rev. Mater.* **2016**, *1* (4), 16013. https://doi.org/10.1038/natrevmats.2016.13.

(14) Li, P.; Kim, H.; Myung, S.-T.; Sun, Y.-K. Diverting Exploration of Silicon Anode into Practical Way: A Review Focused on Silicon-Graphite Composite for Lithium Ion Batteries. *Energy Storage Mater.* **2021**, *35*, 550–576. https://doi.org/10.1016/j.ensm.2020.11.028.

(15) Cheng, X.-B.; Zhang, R.; Zhao, C.-Z.; Zhang, Q. Toward Safe Lithium Metal Anode in Rechargeable Batteries: A Review. *Chem. Rev.* **2017**, *117* (15), 10403–10473. https://doi.org/10.1021/acs.chemrev.7b00115.

(16) Schipper, F.; Erickson, E. M.; Erk, C.; Shin, J.-Y.; Chesneau, F. F.; Aurbach, D. Review—Recent Advances and Remaining Challenges for Lithium Ion Battery Cathodes: I. Nickel-Rich, LiNi $_x$ Co $_y$ Mn $_z$ O $_2$. *J. Electrochem. Soc.* **2017**, *164* (1), A6220–A6228. https://doi.org/10.1149/2.0351701jes.

(17) Liu, Z.; Yu, A.; Lee, J. Y. Synthesis and Characterization of LiNi1−x−yCoxMnyO2 as the Cathode Materials of Secondary Lithium Batteries. *J. Power Sources* **1999**, *81–82*, 416–419. https://doi.org/10.1016/S0378-7753(99)00221-9.

(18) Purwanto, A.; Yudha, C. S.; Ubaidillah, U.; Widiyandari, H.; Ogi, T.; Haerudin, H. NCA Cathode Material: Synthesis Methods and Performance Enhancement Efforts. *Mater. Res. Express* **2018**, *5* (12), 122001. https://doi.org/10.1088/2053-1591/aae167.

(19) Padhi, A.; Nanjudaswamy, K.; Goodenough, J. Phospho-olivines as Positive-Electrode Materials for Rechargeable Lithium Batteries. *J. Electrochem. Soc. 144* (4).

(20) Opetal, J. *Sodium-ion batteries from CATL and BYD to be installed in mass-produced cars by Q4 2023*. https://carnewschina.com/2023/04/20/catl-and-byd-sodium-ion-batteries-will-be-put-into-a-mass-produced-car-in-q4-2023/.

(21) Walter, M.; Kovalenko, M. V.; Kravchyk, K. V. Challenges and Benefits of Post-Lithium-Ion Batteries. *New J. Chem.* **2020**, *44* (5), 1677–1683. https://doi.org/10.1039/C9NJ05682C.

(22) Kubota, K.; Dahbi, M.; Hosaka, T.; Kumakura, S.; Komaba, S. Towards K-Ion and Na-Ion Batteries as "Beyond Li-Ion." *Chem. Rec.* **2018**, *18* (4), 459–479. https://doi.org/10.1002/tcr.201700057.

(23) Li, Y.; Lu, J. Metal–Air Batteries: Will They Be the Future Electrochemical Energy Storage Device of Choice? *ACS Energy Lett.* **2017**, *2* (6), 1370–1377. https://doi.org/10.1021/acsenergylett.7b00119.

(24) Han, X.; Li, X.; White, J.; Zhong, C.; Deng, Y.; Hu, W.; Ma, T. Metal–Air Batteries: From Static to Flow System. *Adv. Energy Mater.* **2018**, *8* (27), 1801396. https://doi.org/10.1002/aenm.201801396.

(25) Sánchez-Díez, E.; Ventosa, E.; Guarnieri, M.; Trovò, A.; Flox, C.; Marcilla, R.; Soavi, F.; Mazur, P.; Aranzabe, E.; Ferret, R. Redox Flow Batteries: Status and Perspective towards Sustainable Stationary Energy Storage. *J. Power Sources* **2021**, *481*, 228804. https://doi.org/10.1016/j.jpowsour.2020.228804.

(26) Neudecker, B. J.; Dudney, N. J.; Bates, J. B. "Lithium-Free" Thin-Film Battery with In Situ Plated Li Anode. *J. Electrochem. Soc.* **2000**, *147* (2), 517. https://doi.org/10.1149/1.1393226.

(27) Huang, W.; Zhao, C.; Wu, P.; Yuan, H.; Feng, W.; Liu, Z.; Lu, Y.; Sun, S.; Fu, Z.; Hu, J.; Yang, S.; Huang, J.; Zhang, Q. Anode-Free Solid-State Lithium Batteries: A Review. *Adv. Energy Mater.* **2022**, *12* (26), 2201044. https://doi.org/10.1002/aenm.202201044.

(28) Nanda, S.; Bhargav, A.; Manthiram, A. Anode-Free, Lean-Electrolyte Lithium-Sulfur Batteries Enabled by Tellurium-Stabilized Lithium Deposition. *Joule* **2020**, *4* (5), 1121–1135. https://doi.org/10.1016/j.joule.2020.03.020.

(29) Zhang, J.; Khan, A.; Liu, X.; Lei, Y.; Du, S.; Lv, L.; Zhao, H.; Luo, D. Research Progress of Anode-Free Lithium Metal Batteries. *Crystals* **2022**, *12* (9), 1241. https://doi.org/10.3390/cryst12091241.

(30) Betz, J.; Bieker, G.; Meister, P.; Placke, T.; Winter, M.; Schmuch, R. Theoretical versus Practical Energy: A Plea for More Transparency in the Energy Calculation of Different Rechargeable Battery Systems. *Adv. Energy Mater.* **2019**, *9* (6), 1803170. https://doi.org/10.1002/aenm.201803170.

(31) Nanda, S.; Gupta, A.; Manthiram, A. Anode-Free Full Cells: A Pathway to High-Energy Density Lithium-Metal Batteries. *Adv. Energy Mater.* **2021**, *11* (2), 2000804. https://doi.org/10.1002/aenm.202000804.

(32) Pal, S.; Zhang, X.; Babu, B.; Lin, X.; Wang, J.; Vlad, A. Materials, Electrodes and Electrolytes Advances for next-Generation Lithium-Based Anode-Free Batteries. *Oxf. Open Mater. Sci.* **2022**, *2* (1), itac005. https://doi.org/10.1093/oxfmat/itac005.

(33) Li, G. Regulating Mass Transport Behaviour for High-Performance Lithium Metal Batteries and Fast-Charging Lithium-Ion Batteries. *Adv. Energy Mater.* **2021**, *11* (7), 2002891. https://doi.org/10.1002/aenm.202002891.

(34) SLAC, C. office. *Study Finds a Way to Prevent Fires in Next-Generation Lithium Batteries*. https://www6.slac.stanford.edu/news/2015-06-17-study-finds-way-prevent-fires-next-generation-lithium-batteries (accessed 2023-05-03).

(35) Assegie, A. A.; Cheng, J.-H.; Kuo, L.-M.; Su, W.-N.; Hwang, B.-J. Polyethylene Oxide Film Coating Enhances Lithium Cycling Efficiency of an Anode-Free Lithium-Metal Battery. *Nanoscale* **2018**, *10* (13), 6125–6138. https://doi.org/10.1039/C7NR09058G.

(36) Beyene, T. T.; Bezabh, H. K.; Weret, M. A.; Hagos, T. M.; Huang, C.-J.; Wang, C.-H.; Su, W.-N.; Dai, H.; Hwang, B.-J. Concentrated Dual-Salt Electrolyte to Stabilize Li

Metal and Increase Cycle Life of Anode Free Li-Metal Batteries. *J. Electrochem. Soc.* **2019**, *166* (8), A1501–A1509. https://doi.org/10.1149/2.0731908jes.

(37) Qian, J.; Adams, B. D.; Zheng, J.; Xu, W.; Henderson, W. A.; Wang, J.; Bowden, M. E.; Xu, S.; Hu, J.; Zhang, J.-G. Anode-Free Rechargeable Lithium Metal Batteries. *Adv. Funct. Mater.* **2016**, *26* (39), 7094–7102. https://doi.org/10.1002/adfm.201602353.

(38) Woo, J.-J.; Maroni, V. A.; Liu, G.; Vaughey, J. T.; Gosztola, D. J.; Amine, K.; Zhang, Z. Symmetrical Impedance Study on Inactivation Induced Degradation of Lithium Electrodes for Batteries Beyond Lithium-Ion. *J. Electrochem. Soc.* **2014**, *161* (5), A827–A830. https://doi.org/10.1149/2.089405jes.

(39) Qian, J.; Henderson, W. A.; Xu, W.; Bhattacharya, P.; Engelhard, M.; Borodin, O.; Zhang, J.-G. High Rate and Stable Cycling of Lithium Metal Anode. *Nat. Commun.* **2015**, *6* (1), 6362. https://doi.org/10.1038/ncomms7362.

(40) Yamada, Y.; Yaegashi, M.; Abe, T.; Yamada, A. A Superconcentrated Ether Electrolyte for Fast-Charging Li-Ion Batteries. *Chem. Commun.* **2013**, *49* (95), 11194. https://doi.org/10.1039/c3cc46665e.

(41) Barchasz, C.; Leprêtre, J.-C.; Patoux, S.; Alloin, F. Electrochemical Properties of Ether-Based Electrolytes for Lithium/Sulfur Rechargeable Batteries. *Electrochimica Acta* **2013**, *89*, 737–743. https://doi.org/10.1016/j.electacta.2012.11.001.

(42) Liu, P.; Ma, Q.; Fang, Z.; Ma, J.; Hu, Y.-S.; Zhou, Z.-B.; Li, H.; Huang, X.-J.; Chen, L.-Q. Concentrated Dual-Salt Electrolytes for Improving the Cycling Stability of Lithium Metal Anodes. *Chin. Phys. B* **2016**, *25* (7), 078203. https://doi.org/10.1088/1674-1056/25/7/078203.

(43) Zhang, S. S.; Fan, X.; Wang, C. An In-Situ Enabled Lithium Metal Battery by Plating Lithium on a Copper Current Collector. *Electrochem. Commun.* **2018**, *89*, 23–26. https://doi.org/10.1016/j.elecom.2018.02.011.

(44) Liang, X.; Pang, Q.; Kochetkov, I. R.; Sempere, M. S.; Huang, H.; Sun, X.; Nazar, L. F. A Facile Surface Chemistry Route to a Stabilized Lithium Metal Anode. *Nat. Energy* **2017**, *2* (9), 17119. https://doi.org/10.1038/nenergy.2017.119.

(45) Xu, R.; Cheng, X.-B.; Yan, C.; Zhang, X.-Q.; Xiao, Y.; Zhao, C.-Z.; Huang, J.-Q.; Zhang, Q. Artificial Interphases for Highly Stable Lithium Metal Anode. *Matter* **2019**, *1* (2), 317–344. https://doi.org/10.1016/j.matt.2019.05.016.

(46) Yan, K.; Lu, Z.; Lee, H.-W.; Xiong, F.; Hsu, P.-C.; Li, Y.; Zhao, J.; Chu, S.; Cui, Y. Selective Deposition and Stable Encapsulation of Lithium through Heterogeneous Seeded Growth. *Nat. Energy* **2016**, *1* (3), 16010. https://doi.org/10.1038/nenergy.2016.10.

(47) Zhang, S. S.; Fan, X.; Wang, C. A Tin-Plated Copper Substrate for Efficient Cycling of Lithium Metal in an Anode-Free Rechargeable Lithium Battery. *Electrochimica Acta* **2017**, *258*, 1201–1207. https://doi.org/10.1016/j.electacta.2017.11.175.

(48) Assegie, A. A.; Chung, C.-C.; Tsai, M.-C.; Su, W.-N.; Chen, C.-W.; Hwang, B.-J. Multilayer-Graphene-Stabilized Lithium Deposition for Anode-Free Lithium-Metal Batteries. *Nanoscale* **2019**, *11* (6), 2710–2720. https://doi.org/10.1039/C8NR06980H.

(49) Belt, J. R.; Ho, C. D.; Miller, T. J.; Habib, M. A.; Duong, T. Q. The Effect of Temperature on Capacity and Power in Cycled Lithium Ion Batteries. *J. Power Sources* **2005**, *142* (1–2), 354–360. https://doi.org/10.1016/j.jpowsour.2004.10.029.

(50) Niu, C.; Lee, H.; Chen, S.; Li, Q.; Du, J.; Xu, W.; Zhang, J.-G.; Whittingham, M. S.; Xiao, J.; Liu, J. High-Energy Lithium Metal Pouch Cells with Limited Anode Swelling and Long Stable Cycles. *Nat. Energy* **2019**, *4* (7), 551–559. https://doi.org/10.1038/s41560-019-0390-6.

(51) Wang, M.; Wang, Q.; Ding, X.; Wang, Y.; Xin, Y.; Singh, P.; Wu, F.; Gao, H. The Prospect and Challenges of Sodium-ion Batteries for Low-temperature Conditions. *Interdiscip. Mater.* **2022**, *1* (3), 373–395. https://doi.org/10.1002/idm2.12040.

(52) Beyene, T. T.; Jote, B. A.; Wondimkun, Z. T.; Olbassa, B. W.; Huang, C.-J.; Thirumalraj, B.; Wang, C.-H.; Su, W.-N.; Dai, H.; Hwang, B.-J. Effects of Concentrated Salt and Resting Protocol on Solid Electrolyte Interface Formation for Improved Cycle Stability of Anode-Free Lithium Metal Batteries. *ACS Appl. Mater. Interfaces* **2019**, *11* (35), 31962–31971. https://doi.org/10.1021/acsami.9b09551.

(53) Louli, A. J.; Genovese, M.; Weber, R.; Hames, S. G.; Logan, E. R.; Dahn, J. R. Exploring the Impact of Mechanical Pressure on the Performance of Anode-Free Lithium Metal Cells. *J. Electrochem. Soc.* **2019**, *166* (8), A1291–A1299. https://doi.org/10.1149/2.0091908jes.

(54) Genovese, M.; Louli, A. J.; Weber, R.; Martin, C.; Taskovic, T.; Dahn, J. R. Hot Formation for Improved Low Temperature Cycling of Anode-Free Lithium Metal Batteries. *J. Electrochem. Soc.* **2019**, *166* (14), A3342–A3347. https://doi.org/10.1149/2.0661914jes.

(55) Alvarez, S. *Tesla, BYD estimated to account for 68% of LFP batteries deployed from Q1-Q3 2022*. https://www.teslarati.com/tesla-byd-68-percent-all-lfp-batteries-deployed-q1-q3-2022-report/ (accessed 2023-04-12).

(56) Nitta, N.; Wu, F.; Lee, J. T.; Yushin, G. Li-Ion Battery Materials: Present and Future. *Mater. Today* **2015**, *18* (5), 252–264. https://doi.org/10.1016/j.mattod.2014.10.040.

(57) Stenina, I.; Minakova, P.; Kulova, T.; Yaroslavtsev, A. Electrochemical Properties of LiFePO4 Cathodes: The Effect of Carbon Additives. *Batteries* **2022**, *8* (9), 111. https://doi.org/10.3390/batteries8090111.

(58) Sun, Y.; Lee, H.-W.; Seh, Z. W.; Liu, N.; Sun, J.; Li, Y.; Cui, Y. High-Capacity Battery Cathode Prelithiation to Offset Initial Lithium Loss. *Nat. Energy* **2016**, *1* (1), 15008. https://doi.org/10.1038/nenergy.2015.8.

(59) Park, K.-S.; Im, D.; Benayad, A.; Dylla, A.; Stevenson, K. J.; Goodenough, J. B. $LiFeO_2$-Incorporated Li_2MoO_3 as a Cathode Additive for Lithium-Ion Battery Safety. *Chem. Mater.* **2012**, *24* (14), 2673–2683. https://doi.org/10.1021/cm300505y.

(60) Huang, C.-J.; Hsu, Y.-C.; Shitaw, K. N.; Siao, Y.-J.; Wu, S.-H.; Wang, C.-H.; Su, W.-N.; Hwang, B. J. Lithium Oxalate as a Lifespan Extender for Anode-Free Lithium Metal Batteries. *ACS Appl. Mater. Interfaces* **2022**, *14* (23), 26724–26732. https://doi.org/10.1021/acsami.2c04693.

(61) James, A. C. W. P.; Goodenough, J. B. Structure and Bonding in Li2MoO3 and Li2−xMoO3 (0 ≤ x ≤ 1.7). *J. Solid State Chem.* **1988**, *76* (1), 87–96. https://doi.org/10.1016/0022-4596(88)90194-6.

(62) Wang, J.; Lakraychi, A. E.; Liu, X.; Sieuw, L.; Morari, C.; Poizot, P.; Vlad, A. Conjugated Sulfonamides as a Class of Organic Lithium-Ion Positive Electrodes. *Nat. Mater.* **2021**, *20* (5), 665–673. https://doi.org/10.1038/s41563-020-00869-1.

(63) Houache, M.; Yim, C.-H.; Karkar, Z.; Abu-Lebdeh, Y. On the Current and Future Outlook of Battery Chemistries for Electric Vehicles—Mini Review. *Batteries* **2022**, *8* (7), 70. https://doi.org/10.3390/batteries8070070.

UNIVERSITÉ CATHOLIQUE DE LOUVAIN
École polytechnique de Louvain
Rue Archimède, 1 bte L6.11.01, 1348 Louvain-la-Neuve, Belgique | **www.uclouvain.be/epl**